

## Cross-match between the latest Swift-BAT and Fermi-LAT catalogs

NAOMI TSUJI,<sup>1</sup> HIROKI YONEDA,<sup>2</sup> YOSHIYUKI INOUE,<sup>3,4,5</sup> TSUGUO ARAMAKI,<sup>6</sup> GEORGIA KARAGIORGI,<sup>7</sup>  
RESHMI MUKHERJEE,<sup>7</sup> AND HIROKAZU ODAKA<sup>8,5</sup>

<sup>1</sup>*Interdisciplinary Theoretical & Mathematical Science Program (iTHEMS), RIKEN, 2-1 Hirosawa, Wako, Saitama 351-0198, Japan*

<sup>2</sup>*RIKEN, Nishina Center, 2-1 Hirosawa, Wako, Saitama 351-0198, Japan*

<sup>3</sup>*Department of Earth and Space Science, Graduate School of Science, Osaka University, Toyonaka, Osaka 560-0043, Japan*

<sup>4</sup>*Interdisciplinary Theoretical & Mathematical Science Program (iTHEMS), RIKEN, 2-1 Hirosawa, Saitama 351-0198, Japan*

<sup>5</sup>*Kavli Institute for the Physics and Mathematics of the Universe (WPI), The University of Tokyo, Kashiwa 277-8583, Japan*

<sup>6</sup>*Northeastern University, 360 Huntington Ave, Boston, MA 02115, USA*

<sup>7</sup>*Columbia University, New York, NY, 10027, USA*

<sup>8</sup>*Department of Physics, The University of Tokyo, 7-3-1 Hongo, Bunkyo, Tokyo 113-0033, Japan*

### ABSTRACT

We report the results of a cross-match study between the hard X-ray and GeV gamma-ray catalogs, by making use of the latest 105-month *Swift*-BAT and 10-yr *Fermi*-LAT catalogs, respectively. The spatial cross-matching between the two catalogs results in the matching of 132 point-like sources, including  $\sim 5\%$  of false-match sources. Additionally, 24 sources that have been identified as the same identifications are matched. Among the 75 extended sources in the *Fermi*-LAT catalog, 31 sources have spatial coincidences with at least one *Swift*-BAT source inside their extent. All the matched sources consist of blazars ( $> 60\%$ ), pulsars and pulsar wind nebulae ( $\sim 13\%$ ), radio galaxies ( $\sim 7\%$ ), binaries ( $\sim 5\%$ ), and others. Compared to the original catalogs, the matched sources are characterized by a double-peaked photon index distribution, higher flux, and larger gamma-ray variability index. This difference arises from the different populations of sources, particularly the large proportion of blazars (i.e., FSRQ and BL Lac). We also report 13 cross-matched and unidentified sources. The matched sources in this study would be promising in the intermediate energy band between the hard X-ray and GeV gamma-ray observations, that is the unexplored MeV gamma-ray domain.

**Keywords:** catalogs — X-rays: general — gamma rays: general — galaxies: active

### 1. INTRODUCTION

The sky in the MeV gamma-ray energy range has remained unexplored for almost 30 years since the first devoted MeV detector, the Imaging Compton Telescope COMPTEL onboard the Compton Gamma-Ray Observatory (CGRO) mission (Schoenfelder et al. 1993) launched in April 5, 1991, was in operation. However, there are promising discoveries to be made in this energy band (Takahashi et al. 2013), which is the main motivation for sensitive and improved observations in the next decades. While MeV observations await the next-generation instruments, the neighboring energy bands, the hard X-ray and the GeV gamma ray, have been well studied for the last decade by, for example,

*Swift*/Burst Alert Telescope (BAT) (Barthelmy et al. 2005) and *Fermi*/Large Area Telescope (LAT) (Atwood et al. 2009), respectively. These two observatories provide us with a legacy of observational data, including source catalogs, in the corresponding energy channels. Therefore, by using the latest *Swift*-BAT and *Fermi*-LAT catalogs, one can perform catalog cross-match and somewhat predict the currently unavailable information in the MeV band.

The importance of the catalog cross-match is to list promising objects in the MeV gamma-ray band. Sources that have been detected both in the hard X-ray and GeV gamma ray would be plausible MeV gamma-ray emitting sources unless the X-ray and gamma-ray photon indices are extremely soft and hard, respectively. This new catalog of the cross-matched sources is useful for ongoing projects for the MeV observations (e.g., De An-

gelis et al. 2018; McEnery et al. 2019; Tomsick et al. 2019; Aramaki et al. 2020).

The cross-match between the hard X-ray and GeV gamma-ray catalogs is also meaningful in high energy astrophysics. Both these energy ranges point to non-thermal radiation processes, as we expect that the thermal X-ray emission does not have a substantial contribution to the hard X-ray. Thus, the hard X-rays originate from synchrotron radiation or inverse Compton (IC) scattering from accelerated electrons, while the gamma-rays are produced by a leptonic process (i.e., IC scattering from high-energy electrons) or a hadronic process (e.g., hadronuclear interaction). An alternative is non-thermal bremsstrahlung from accelerated particles. If a source emits both the hard X-rays and GeV gamma rays that originate from accelerated particles (electrons or protons) via the same or different radiation mechanisms, the broadband energy spectrum gives us an important clue to understand the particle acceleration and/or the emission mechanisms.

Maselli et al. (2011) previously performed a catalog cross correlation using the 54-month *Swift*-BAT catalog (2PBC; Cusumano et al. (2010)) and the 1-yr *Fermi*-LAT catalog (1FGL; Abdo et al. (2010)), which had 1256 and 1451 entries, respectively. In this paper, we revisit to the cross-matching by making use of the latest catalogs; the 105-month *Swift*-BAT catalog (Oh et al. 2018) and the 10-yr *Fermi*-LAT catalog (4FGL-DR2; Ballet et al. (2020)). With the more accumulated data and better flux sensitivity, the number of sources in the latest catalogs were improved. Both catalogs were based on the observational data of all sky surveys. *INTEGRAL* (Winkler et al. 2003) also performed hard X-ray observations and provided us with a hard X-ray catalog (see, e.g., Bird et al. 2016). However, because of its non-uniform exposure toward the sky (e.g., *INTEGRAL* has deeper exposure on the Galactic plane), we complementarily use the *INTEGRAL* catalog in this study.

In this work, we present a catalog cross-match using the latest *Swift*-BAT and *Fermi*-LAT catalogs. Section 2 briefly summarizes the two catalogs. The matching method is given in Section 3. The results of the matched sources are presented in Section 4. In Section 5, we compare the matched catalog with other existing catalogs in the energy bands from hard X-ray to MeV gamma ray, investigate properties of the matched sources, and discuss the unidentified sources. The conclusions are presented in Section 6.

## 2. CATALOGS

This work makes use of the *Swift*-BAT 105-month (Oh et al. 2018) and the *Fermi*-LAT fourth (Data Release-

2) (Abdollahi et al. 2020; Ballet et al. 2020) catalogs of hard X-ray and GeV gamma-ray sources, respectively.

### 2.1. *Swift*-BAT 105-month catalog

The Neil Gehrels Swift Observatory (*Swift*) started its operation after the spacecraft was launched on November 20, 2004 (Gehrels et al. 2004). There are three scientific instruments onboard, UV/Optical Telescope (UVOT; 170–650 nm), X-ray Telescope (XRT; 0.2–10 keV), and Burst Alert Telescope (BAT; 14–195 keV). BAT consists of a coded-aperture mask and a large-area solid state detector (CdZnTe) array, enabling us to detect hard X-rays in the 15–150 keV energy band with a large field of view (FoV) of 1.4 sr and a point spread function (PSF) of 17' (Barthelmy et al. 2005).

Although BAT is primarily designed for detecting gamma-ray bursts (GRBs), the accumulated data allows the BAT team to perform a uniform all-sky survey and produce a hard X-ray source catalog. The latest catalog, the *Swift*-BAT 105-month catalog (Oh et al. 2018), made use of data taken from December of 2004 to August of 2013. Using the 105-month data, the all sky in the 14–195 keV band was uniformly covered with sensitivities of  $8.40 \times 10^{-12}$  erg cm $^{-2}$  s $^{-1}$  and  $7.24 \times 10^{-12}$  erg cm $^{-2}$  s $^{-1}$  for over 90% and 50% of the sky, respectively. This resulted in detection of 1632 sources at  $> 4.8\sigma$ . Images, 8-channel energy spectra, and month-scale light curves of the sources in the catalog are available<sup>1</sup>. In the *Swift*-BAT 105-month catalog, the largest proportion is Seyfert galaxies (827 in total; including 379 Seyfert I and 448 Seyfert II), the second one is X-ray binaries (225 in total; 109 low mass X-ray binaries (LMXBs), 108 high mass X-ray binaries (HMXBs), and 8 others), and the third one is beamed active galactic nuclei (AGNs) (158 in total; including flat spectrum radio quasars (FSRQs) and BL Lac types (BLLs)).

### 2.2. *Fermi*-LAT 4FGL-DR2 catalog

The *Fermi* satellite, launched on June 11, 2008, consists of two scientific instruments, Large Area Telescope (LAT) and Gamma-ray Burst Monitor (GBM). The *Fermi*-LAT is a pair-conversion gamma-ray telescope with a precision tracker and calorimeter, each consisting of a 4×4 array of 16 modules, a segmented anti-coincidence detector that covers the tracker array, and a programmable trigger and data acquisition system (Atwood et al. 2009). *Fermi*-LAT enables us to perform spectroscopy in gamma-ray energies ranging from 20 MeV to more than 300 GeV with a wide FoV of 20%

<sup>1</sup> <https://swift.gsfc.nasa.gov/results/bs105mon/>

of the sky. The PSF of *Fermi*-LAT is approximately  $3.5^\circ$  at 100 MeV and  $0.1^\circ$  at 10 GeV. The other instrument, GBM, covers two thirds of the sky at a moment and detects GRBs in the 8 keV–40 MeV band.

*Fermi*-LAT 4th Catalog Data Release 2 (4FGL-DR2<sup>2</sup>; Ballet et al. (2020)) is the latest catalog based on 10-yr observational data taken from August 4, 2008 to August 2, 2018. The previous catalog, the 8-yr *Fermi*-LAT 4th catalog (4FGL<sup>3</sup>), was described in detail in Abdollahi et al. (2020). These catalogs made use of the data of the all-sky survey with the flux sensitivity of  $10^{-11}$ – $10^{-12}$  erg cm<sup>-2</sup> s<sup>-1</sup> in the energy range of 50 MeV to 1 TeV, depending on the source location and the energy of gamma rays. 4FGL-DR2 has 5788 sources detected at  $> 4\sigma$ , while 4FGL has 5065 sources. In both catalogs, 75 sources were reported to have spatial extension. The catalogs provide us with the locations, 7-band energy spectra, and lightcurves in 2-month and 1-yr time bins<sup>4</sup>, which are useful for cross-matching in this paper. We mainly made use of 4FGL-DR2 for the following analyses and used 2-month lightcurves of 4FGL for reference since 4FGL-DR2 did not include 2-month lightcurves. The three biggest source types in 4FGL-DR2 are blazars (60%), unknown or unidentified sources (30%), and pulsars (5%).

Here we note that the source category defined in the *Fermi*-LAT catalog has two cases, an upper case (e.g., FSRQ) and a lower case (e.g., fsrq), which respectively indicate a firm association and an association. Throughout this paper, we also adopt the same definition for the source category of 4FGL-DR2, otherwise mentioned.

### 3. CROSS-MATCH – METHOD

We cross-match the 1632 *Swift*-BAT sources and the 5788 *Fermi*-LAT sources by a spatially matching for point-like sources (Section 3.1) and extended sources (Section 3.2) and carry out an identification matching (Section 3.3). It should be noted that we use coordinates of the detected sources, not coordinates of the associated sources, in order to calculate the angular separation between the BAT and LAT sources.

#### 3.1. Spatial cross-match of point sources

The separation threshold for spatial cross-match ( $0.08^\circ$ ) was determined in the same way proposed in Itoh et al. (2020). First, we produced a distance profile, which is a sum of the number of the *Fermi*-LAT

sources located between  $r$  and  $r + dr$  centered at each *Swift*-BAT source as a function of the distance  $r$  (Figure 1). In Figure 1,  $dr$  is set to be  $0.02^\circ$ , and the profile is generated up to  $r = 2.0^\circ$ . The distance profile contained a spike around  $r = 0^\circ$  and a linear increase for  $r > 0.2^\circ$ . The former feature indicates plausible associations, while the latter could correspond to false matches. We thus fit the linearly increasing profile at  $r > 0.2^\circ$  with an empirical model of  $N = ar dr$ , where  $a$  is a constant. The best-fit parameter of  $a$  was obtained to be 2500 counts deg<sup>-2</sup>. In order to suppress the false associations (i.e., the background level) down to 5%, we set the separation threshold,  $r_{\text{sep}}$ , to  $0.08^\circ$ . Note that the background level of 10% corresponded to  $r_{\text{sep}}$  of  $0.12^\circ$ . We checked that the choices of  $dr$  and the  $r$  range for the distance profile did not have effects on determination of  $a$  and  $r_{\text{sep}}$ . The obtained  $r_{\text{sep}}$  ( $=0.08^\circ$ ) is much smaller than the PSFs of the detectors and comparable with the average positional uncertainty that is  $0.062^\circ$  for *Swift*-BAT and  $0.06^\circ$ – $0.08^\circ$  for *Fermi*-LAT.

Applying  $r_{\text{sep}}=0.08^\circ$ , 132 sources were found to be cross-matched (i.e., that had counterparts within the separation). Note that the number of the matched sources increased to 161 sources if we adjusted  $r_{\text{sep}}=0.12^\circ$ , including possible 10% false matches. The 132 spatially matched sources are listed in Table 1, in which we show the source name, source type, position, spectral information (flux and photon index), and gamma-ray time variability index, taken from the original two catalogs. We also show the derived separation and Flag which indicates the status of the matched source (see Section 4.1 for detail). The results are presented in Section 4.1.

It should be noted that the position determination accuracy of both *Swift*-BAT and *Fermi*-LAT depends on brightness of sources. Therefore we also carried out a spatial cross-match by setting the separation threshold to  $\sigma_{\text{BAT}} + \sigma_{\text{LAT}}$ , where  $\sigma_{\text{BAT}}$  and  $\sigma_{\text{LAT}}$  indicate the positional error of each source in the *Swift*-BAT and *Fermi*-LAT catalogs, respectively. This results in detection of 182 matched sources, which includes all the 132 spatially matched sources. Among the 50 sources that are missed in the spatial matching by  $r_{\text{sep}}=0.08^\circ$ , 27 sources are matched extended sources (Section 3.2) or identification-matched sources (Section 3.3), and the remains are 7 unidentified sources and 16 false matches.

#### 3.2. Spatial cross-match of extended sources

The 4FGL-DR2 catalog confirmed 75 extended sources, whose properties, including morphology, were provided in the catalog. The source extensions range from  $0.03^\circ$  to  $3.5^\circ$ . We cross-matched the two cata-

<sup>2</sup> [https://fermi.gsfc.nasa.gov/ssc/data/access/lat/10yr\\_catalog/](https://fermi.gsfc.nasa.gov/ssc/data/access/lat/10yr_catalog/)

<sup>3</sup> [https://fermi.gsfc.nasa.gov/ssc/data/access/lat/8yr\\_catalog/](https://fermi.gsfc.nasa.gov/ssc/data/access/lat/8yr_catalog/)

<sup>4</sup> Note that 2-month lightcurves are available only in 4FGL (the 8-yr catalog).

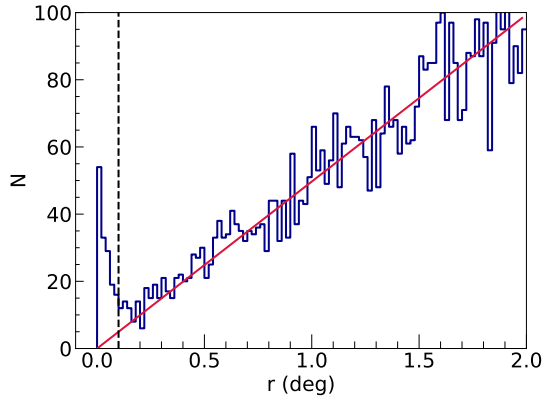


**Figure 1.** Distance profile in the range of  $r = 0\text{--}2^\circ$  with  $dr = 0.02^\circ$ . The red line shows the best-fit background model, with  $a$  being 2500 counts  $\text{deg}^{-2}$ . The black dashed vertical line indicates the separation threshold of  $0.08^\circ$ , which suppresses the background level to 5%.

logs based on the assumption that the extended LAT sources had BAT sources within their extension. 29 sources were matched with  $d \leq \sigma_\gamma$ , where  $d$  is the angular separation between the center of the LAT source and the nearest BAT source, and  $\sigma_\gamma$  is the gamma-ray spatial extent (see Abdollahi et al. 2020, for details). Additional 2 sources (Large Magellanic Cloud (LMC) 30 Dor. West and HESS J1420–607) were matched with  $d + \sigma_{\text{BAT}} \leq \sigma_\gamma$ , taking the positional error of the BAT source ( $\sigma_{\text{BAT}}$ ) into consideration. In this paper, we defined these 31 sources as extended cross-matched sources. It is notable that MSH 15–52 and Crab nebula (IC component), which were extended sources in 4FGL-DR2, were also positionally matched in Section 3.1.

### 3.3. Source identification cross-match

We also used an identification matching method to cross-match sources. When we cross-matched by the source names provided in the catalogs, 123 were matched between the *Swift*-BAT and *Fermi*-LAT catalogs. 94 of these 123 sources were already included in the spatial match of point sources (Section 3.1 and Table 1), and another 5 sources were already presented in the spatial match of extended sources (Section 3.2 and Table 2), so we do not include them here. The remaining 24 sources were not contained in our method of spatial cross-match. Among the spatially unmatched and name-matched 24 sources, 10 were spatially matched if we adopted  $r_{\text{sep}}=0.12^\circ$  in Section 3.1. The remaining 14 sources may have been positionally unmatched because they had relatively large position errors because of the faint flux and had slightly larger separation than  $r_{\text{sep}}$ . The separation was remarkably large for the galactic two

pulsars, PSR J1420–6048 and PSR J1723–2837, and they had large position uncertainties because of their location in a complex region on the Galactic plane.

To search for associated sources in 4FGL-DR2, the 105-month *Swift*-BAT catalog was utilized as well as the many other catalogs listed in Table 6 of Abdollahi et al. (2020). In fact 4FGL-DR2 included 5 sources which were registered solely from the *Swift*-BAT catalog and not from the other catalogs in Table 6 in Abdollahi et al. (2020). They were included in our matched catalog, No. 131, 132, and 154–156 in Table 1. The former two were spatially matched with in  $r_{\text{sep}}=0.08^\circ$ , while the latter three were matched by the identifications. It should be noted that the latter three sources had small association probability,  $P < 0.6$  (see Abdollahi et al. 2020, for details), except for SWIFT J1808.5–3655.

## 4. RESULTS — CROSS-MATCHED CATALOG

The catalog of the cross-matched sources between the *Swift*-BAT and *Fermi*-LAT is provided here. The spatial cross-match resulted in 132 matched sources, while the identification cross-match resulted in 24 more matched sources. All the 156 matched point-like sources are summarized in Table 1 and discussed in Section 4.1, and the cross-matched extended sources are listed in Table 2 (Section 4.2). Section 4.3 presents the summary of source types of the matched sources. It should be noted that Crab (No. 116 in Table 1) has three entries in 4FGL-DR2 (i.e., emission from the Crab pulsar, synchrotron emission from the Crab nebula, and inverse Compton scattering from the Crab nebula). In this paper, we have listed only the synchrotron component that represents the three entries, because it corresponds to the hard X-ray emission seen by BAT.

### 4.1. Cross-matched point sources

The obtained 156 sources in Table 1 were divided into five groups: firmly matched source (with Flag being M in Table 1), false-matched source (F), source with different source categories between the two catalogs (D), unidentified source or unknown association (U), and ambiguous source (A). Brief descriptions of each group are given in the following.

*Matched source (Flag=M)*—The matched source was defined as a source which was identified as the same source name and the same source type between the *Swift*-BAT and *Fermi*-LAT catalogs.

*False match (Flag=F)*—The false match indicates that a spatially matched source had different identifications and different source types in the two catalogs. Because  $r_{\text{sep}}=0.08^\circ$  was determined as the level of false



matching was reduced to 5%, the 132 spatially matched sources would contain roughly 7 falsely matched sources. Indeed, Table 1 includes 8 sources where the two associated sources are not identical in the two catalogs. Among the 8 sources, 3 sources were pulsars in 4FGL-DR2 but different point sources in the BAT catalog (No. 108, 109, and 114 in Table 1). One source was classified as a pulsar wind nebula (PWN) in 4FGL-DR2 but a molecular cloud in the BAT catalog (No. 117), resulting from the fact that both sources are located in the radio arc near the complex galactic center. The rest 4 false-match sources were globular clusters in 4FGL-DR2, but the corresponding BAT sources were LMXBs in the globular clusters (No. 125–127 and 129). These sources were likely false-matched because (1) they were confused by the emission from the Galactic plane ( $|b| < 10^\circ$  for No. 108, 109, 117, 127, and 129), (2) they were relatively faint and had large uncertainty in position determination accuracy (No. 125 and 126), or (3) they had slightly smaller separation than  $r_{\text{sep}}$  (No. 114).

*Different source type (Flag=D)*—The different-type source is identified as a source which has the same source name, but has different source types defined in the two catalogs. Table 1 includes 11 of these sources. 7 sources were AGNs with different subclasses defined in the two catalogs: they were Seyfert galaxies in the BAT catalog, but in 4FGL-DR2 they were classified as blazar candidate of uncertain type (bcu) (No. 81 in Table 1), radio galaxies (No. 95, 96, 149 and 150), or starburst galaxies (No. 98 and 100). They had the different subclasses because the hard X-ray and GeV gamma-ray radiation would originate from the same AGN but from the different mechanism. We can naturally expect such associations. The X-ray emission in Seyfert galaxies originates in AGN coronae, which do not emit intense GeV gamma-ray emission due to internal  $\gamma\gamma$  annihilation (Inoue et al. 2019, 2020). Since Seyfert galaxies also have star-formation activity, we see GeV emission from some of nearby Seyfert galaxies (e.g., Ackermann et al. 2012). In radio galaxies, the X-ray emission originates in the same way as in Seyfert galaxies, while AGN jet can dominate the gamma-ray emission (Kataoka et al. 2011). Another different-category sources were supernova remnants (SNRs) in the BAT catalog but pulsars in 4FGL-DR2 (No. 106 and 107), and they were known SNRs hosting pulsars (e.g., Ferrand & Safi-Harb 2012; Araya & Herrera 2021; Hitomi Collaboration et al. 2018). 1RXS J122758.8-485343 (No. 110) was classified as a CV and pulsar in the *Swift*-BAT and *Fermi*-LAT catalogs, respectively. Although the BAT catalog labeled it as a CV, it is also known as a peculiar hard X-ray source possibly associated with the *Fermi*-LAT source. de Mar-

tino et al. (2013), based on the multiwavelength observations from the radio to gamma-ray energy bands, suggested that the system would be a gamma-ray emitting LMXB. Despite the extensive study, the nature of source No. 110 remains undetermined, and thus we labeled this source as Flag=D. The other source, the Galactic center (No. 83), was classified as SGR A\* (source type is Galactic Center) in the BAT catalog and Galactic Centre (source type is bcu) in 4FGL-DR2.

*Unidentified association (Flag=U)*—There were 9 sources with unknown associations, of which the source type was unclear either in the *Swift*-BAT or *Fermi*-LAT catalogs (No. 58, 65, 75, 130–132, and 154–156). It should be noted that 4DFL-DR2 has two-type definitions of uncertain sources; unidentified type (i.e., sources without any firm associations) and unknown type (i.e., low Galactic-latitude sources associated solely by the Likelihood-Ratio method (see Abdollahi et al. 2020, for detail)). 4FGL-DR2 has 1679 unidentified sources and 115 sources of unknown type. In this paper, we merged both types and referred to them as the unidentified sources. These sources, with their spectral energy distributions (SEDs), are discussed in Section 5.3.

*Ambiguous sources (Flag=A)*—Three sources, No. 7, 13, and 76 in Table 1, were flagged as ambiguous, although their source types were AGNs in a broad meaning (i.e., Seyfert galaxy in the BAT catalog, but bl or bcu in 4FGL-DR2). If the associations defined in the two catalogs are correct, these 3 sources would be false-matched. However, the separation was smaller than the accuracy of position determination, and it might be better not to conclude that they were false-matched sources. We, therefore, left them being ambiguous sources, and they need more investigations in the future to determine if they could be false matches or AGNs with different subclass.

#### 4.2. Cross-matched extended sources

All the BAT sources located inside the 31 LAT extended sources are listed in Table 2, and the angular separation for each source from the LAT source is also shown. 12 LAT sources have more than one BAT source within the extent. It should be noted that among the 31 sources, MSH 15–52 was also matched by the spatial matching method (Section 3.1), and RX J1713.7–3946, HESS J1837–069, and HESS J1632–478 were also matched by the identification-matching (Section 3.3). Since they were extended LAT sources, they are omitted in Section 4.1 and discussed in this section.

The breakdown of the 31 matched extended sources is as follows. In the *Fermi*-LAT catalog we had 2 galax-

ies (Small Magellanic Cloud (SMC) and LMC) and 3 unidentified subregions of LMC (Far West, 30 Dor West, and North of LMC). Although they were positionally coincident with some HMXBs and a pulsar, the extended gamma rays are not associated with these point sources, thus setting them to false matches. Additionally, the lobes in Centaurus A detected by LAT were also matched as Centaurus A (radio galaxy) in BAT. 10 PWNe in 4FGL-DR2 were matched with the associated pulsars in the *Swift*-BAT catalog, which are the central compact object of those PWNe. There were 7 extended SNRs matched in our study. Only two of them (RX J1713.7–3946 and RX J0852.0–4622) were known associations, while the other 5 included 3 false-matches (SNR G150.3+04.5, Monoceros, and gamma Cygni), one unknown association (Sim 147), and one ambiguous source (SNR G337.0–00.1 which hosted SGR 1627–41 (a magnetar) and IGR J16358–4726 (a pulsar) within its extent). Cygnus X was the only one star forming region among the matched extended sources, and within the gamma-ray extent it contained Cyg X-3 (HMXB) and 2 AGNs. This, however, was falsely matched because the extended gamma-ray emission from the star forming region did not originate from those point sources. Among the five matched spp<sup>5</sup>, 3 (HESS J1632–478, HESS J1813–178, and Kes 73) were plausible associations between SNR or PWN in gamma-ray and SNR or pulsar in X-ray. W 41, having a star SWIFT J1834.9–0846 measured by BAT, could be a possible false-match source. We left HESS J1809–193 as an ambiguous source because of the association with PSR J1811–1925, according to the spatial coincidence reported in [H. E. S. S. Collaboration et al. \(2018\)](#). Furthermore, there were 3 unidentified extended *Fermi*-LAT sources (FGES J1036.3–5833, FGES J1409.1–6121, and HESS J1808–204), which had BAT counterparts within their extended sources radii. As mentioned above, Sim 147 that was matched with an unknown BAT source, SWIFT J053457.91+282837, could be also an unidentified source. These 4 unidentified sources will be discussed in 5.

#### 4.3. Summary of the matched sources

The source type summary of the matched sources is presented in the form of the *Swift*-BAT and *Fermi*-LAT definitions, respectively, in Table 4 and Table 5. Figure 2 indicates the source type fraction of the matched sources compared to the original catalogs. Note that only firmly matched sources (i.e., Flag is M or D in Table 1 and Table 2) are shown in Figure 2.

In the *Swift*-BAT 105-month catalog, the biggest population was Seyfert galaxy, which however was not a common source category in 4FGL-DR2, resulting in a few cases of the matched Seyfert galaxies in this study. 8 BAT Seyfert galaxies were matched, while the number reduced to 2 in the source definition of *Fermi*-LAT. Most of Seyfert galaxies defined in the *Swift*-BAT catalog were matched with other types of AGNs, such as bcu, radio galaxy, or starburst galaxy, as labeled as Flag=D (see Section 4.1). The second largest proportion in the *Swift*-BAT catalog was X-ray binaries (HMXB, LMXB, and XRB<sup>6</sup>). In this work, the fraction of the matched HMXBs was roughly comparable with that of the original catalog, although LMXBs which occupied the same fraction in the original catalog were hardly matched. However, the numbers of the matched HMXB and LMXB were small (i.e., five HMXBs and one LMXB), and thus it did not allow us further discussion about the fraction. We note that the matched HMXBs were well known binary systems, such as LS 5039 and Cyg X-1, and two LMXBs classified as the unidentified sources (SAX J1808.4–3658 and XTE J1652–453) could be possible candidates of the matched sources (see Section 5.3 for details). The beamed AGNs, which were the third largest population in the original catalog, dominate in this matched catalog. It is worth noting that the second biggest population in our catalog was pulsars, which was a minor class in the *Swift*-BAT catalog. Some of the *Swift*-BAT pulsars were matched with their nebulae in 4FGL-DR2.

In both the *Fermi*-LAT and our matched catalogs, the most predominant source class was blazars. Particularly in our catalog, the fraction of BLLs was compatible with that of the original catalog, while more FSRQs were matched. This is ascribed to that FSRQs could be easily detected by *Swift*-BAT because of the typically hard spectrum in the X-ray energy range ([Toda et al. 2020](#)). The number of the matched bcu appeared small compared to the original catalog. In 4FGL-DR2, the number of the unidentified sources was remarkably numerous, but they were not included in our catalog. We found 9 cross-matched unidentified sources in total, most of which needed more investigation to confirm the association with the hard X-ray (see Section 5.3 and Section 5.4). The third largest population in 4FGL-DR2 was pulsars, and we also had similar fraction of pulsars in our catalog. It should be noted that PWNe and radio galaxies constituted a larger fraction in our catalog,

<sup>6</sup> ‘XRB’ in the *Swift*-BAT catalog indicates other type of X-ray binary (i.e., wind-colliding binary system, such as Eta Carina).

<sup>5</sup> ‘spp’ is defined as a possible SNR or PWN in 4FGL-DR2.

while these two source categories were minor components in the original catalog. All of the matched PWNe, however, were matched with the pulsars in the X-ray but not matched with the nebulae.

107 beamed AGNs in the *Swift*-BAT definition and 98 blazars (FSRQ, BLL, and bcu) in 4FGL-DR2 are firmly identified in our matched catalog. These numbers were roughly consistent with that in Paliya et al. (2019), which reported that 101 BAT blazars were gamma-ray emitting and significantly detected with *Fermi*-LAT. Since Paliya et al. (2019) selected the BAT blazars not based on the original definition of beamed AGN, the number of the blazars were not exactly same with our study. Indeed, 12 blazars in Paliya et al. (2019) did not appear in the our catalog.

## 5. DISCUSSION

We compared our catalog to existing catalogs in the energy range from hard X-ray to sub-GeV gamma-ray, such as the COMPTEL catalog, the *INTEGRAL* catalog, the first *Fermi*-LAT low energy catalog (1FLE), and the previous work by Maselli et al. (2011), in Section 5.1. In Section 5.2, we investigate the property of physical parameters (i.e., photon index, flux, and time variability) of our cross-matched sources. The unidentified point-like and extended sources are discussed in Section 5.3 and Section 5.4, respectively. Finally, we address the meaning of this work toward the future projects of satellites or balloon experiments in Section 5.5.

### 5.1. Comparison with other catalogs

#### 5.1.1. Comparison with COMPTEL catalog

The COMPTEL catalog (Schönfelder et al. 2000) was produced based on the first five-year data in the 0.75–30 MeV energy range. It includes 25 steady sources, 7 line gamma-ray sources, and 31 GRBs. In this paper, we consider the 25 sources that were significantly detected at  $> 3\sigma$ , excluded two of them (High-velocity cloud (HVC) complexes M and A area and HVC complex C) due to the large extent of 20–30°, and added 4 pulsars in Table 3 of Schönfelder et al. (2000). The 27 COMPTEL sources in total are shown in Table 3.

When matching with the COMPTEL catalog, the identification match was the most reasonable, and the spatial match (described in Section 3.1) cannot be applicable because the coordinates of most of COMPTEL sources were taken from their counterparts. However, the position of sources discovered by the CGRO mission (source name starting with ‘GRO’) was determined by the COMPTEL observations. We, thus, can apply the spatial match method to these sources.

First, we conducted a name-match method to the all COMPTEL sources and searched for counterparts in the *Swift*-BAT and *Fermi*-LAT catalogs. For the identification-unmatched sources, we also picked up the nearest sources from the *Swift*-BAT and *Fermi*-LAT catalogs, and then set a separation threshold of  $1^\circ$  for positional matching. It should be noted that COMPTEL has the source location accuracy of  $\sim 1^\circ$  and the angular resolution of 3–5°.

The results of cross-matching are described in Table 3. Among the 27 COMPTEL sources, 16 sources were included in our *Swift*-BAT and *Fermi*-LAT cross-matching and the corresponding source No. of Table 1 and Table 2 is given in Table 3. The following 5 sources were matched with 4FGL-DR2 but not with the BAT catalog: PSR J0633+1746 (a.k.a. Geminga; No. 3 in Table 3), PSR B0656+14 (No.4), PSR B1055–52 (No. 6), Vela/Carina (an unidentified extended emission; No. 14), and PKS 0208–512 (No. 22). The former 3 pulsars appeared faint in hard X-ray energy band. For Nova Per 1992 (No. 12), an X-ray transient, there was no *Swift*-BAT and *Fermi*-LAT counterparts. The remaining 5 sources were ambiguous: GRO J2227+61 (No. 10), GRO J0516–609 (No. 20), GRO J1753+57 (No. 25), GRO J1040+48 (No. 26), and GRO J1214+06 (No. 27). Since there were no *Swift*-BAT and *Fermi*-LAT counterparts within  $1^\circ$ , the position determination accuracy of COMPTEL, around GRO J1753+57 (No. 25) and GRO J1040+48 (No. 26), these two sources would be unmatched. Indeed, Schönfelder et al. (2000) suggested that the emission from GRO J1753+57 could be modelled as a combination of emission from both GRO J1837+59 (a bright unidentified EGRET source) and the steep spectrum EGRET blazar QSO 1739+522. GRO J2227+61 (No. 10) had SWIFT J2221.6+5952 and PSR J2229+6114 located  $1.7^\circ$  and  $0.16^\circ$  away from the COMPTEL emission. GRO J0516–609 (No. 20) that was an unknown flaring source (Bloemen et al. 1995) had a *Fermi*-LAT source, PMN J0507–6104, within  $1.03^\circ$ . GRO J1214+06 (No. 27) had two possible counterparts, 2MASX J12150077+0500512 and SDSS J12168+0541 located  $0.495^\circ$  and  $0.567^\circ$  away from the COMPTEL emission, respectively.

#### 5.1.2. Comparison with INTEGRAL-IBIS catalog

The *INTEGRAL* observatory, launched on October 17 of 2002, consists of two main scientific instruments, the gamma-ray spectrometer SPI and the gamma-ray imager IBIS, and two sub instruments, the two X-ray monitors JEM-X and the optical monitoring camera OMC (Winkler et al. 2003). The accumulated data taken by one of the main instruments, the coded mask telescope

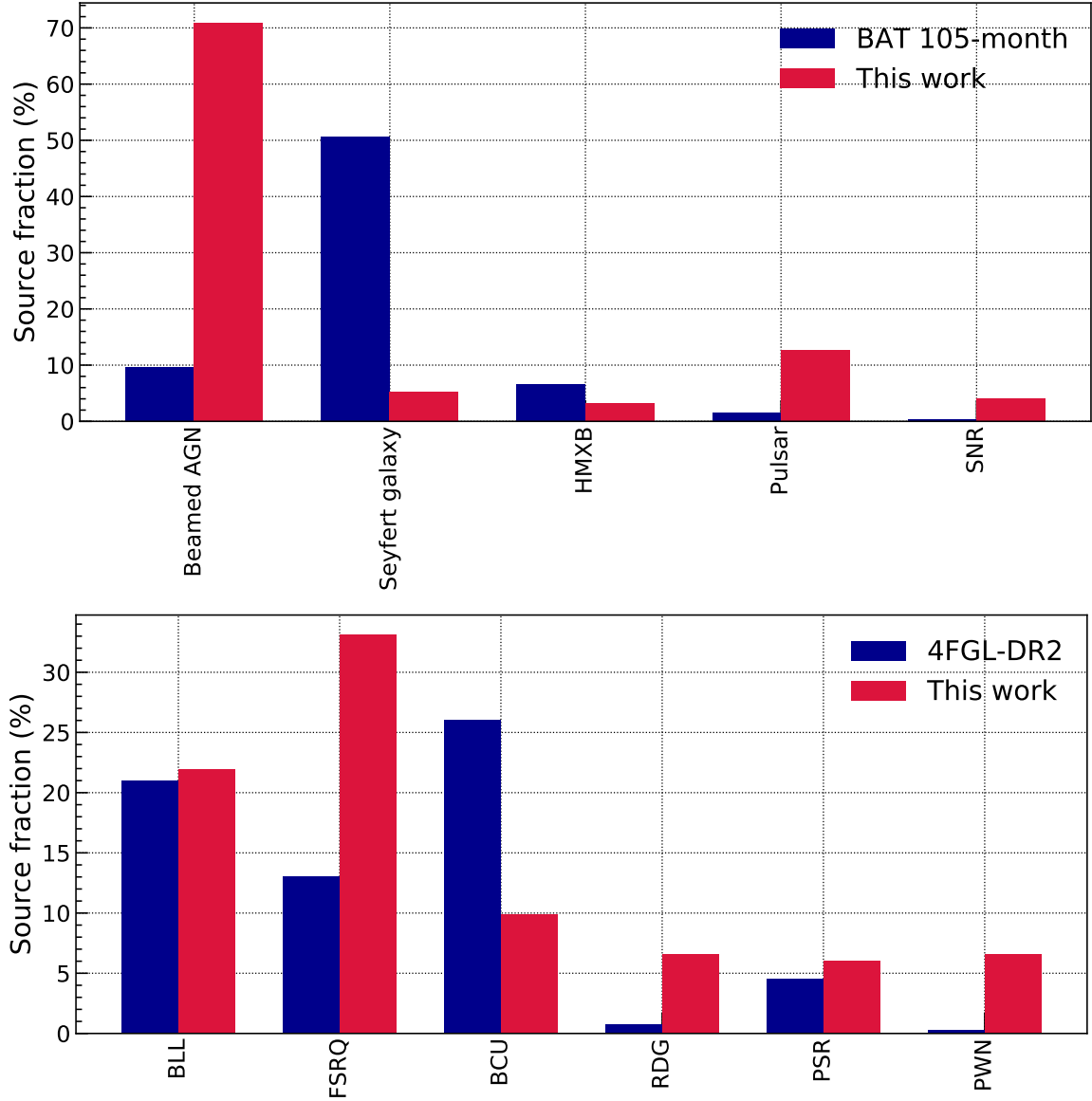


**Figure 2.** Top: Source type fraction of the matched catalog and the *Swift*-BAT catalog. Bottom: Same as top for the *Fermi*-LAT catalog. Note that the source category includes associations with small letters (i.e., BLL includes BLL and bl). Only source types with the number of the matched sources of  $\geq 6$  and  $\geq 9$  are shown for the *Swift*-BAT and *Fermi*-LAT catalogs, respectively.

IBIS (particularly ISGRI, the low energy array on IBIS with a pixelated CdTe detector; [Ubertini et al. \(2003\)](#)), allows us a survey in the energy range from 15 keV to 1 MeV. Using the 1000-orbit data taken from 2002 to 2010 ( $\sim 110$  Ms), [Bird et al. \(2016\)](#) provided the 4th *INTEGRAL*-IBIS catalog, which contained 939 sources detected at  $> 4.5\sigma$  in the 17–100 keV energy range. The latest IBIS catalog (version 43<sup>7</sup> released on September

13 of 2019) contains 1227 entries with ‘ISGRI\_FLAG’ of  $> 1$ , and it was used in the following.

First, we matched the latest IBIS catalog with the 105-month *Swift*-BAT catalog. Using the same method as in Section 3.1 resulted in  $r_{\text{sep}}=0.26^\circ$ , which is relatively large compared to the position uncertainty of BAT and IBIS. The large value of  $r_{\text{sep}}$  could be attributed to the fact that the distance profile of the BAT-IBIS catalog cross-match has characteristic features of a sharpened peak (i.e., the angular separation between each BAT source and the closest IBIS source is more concentrated

<sup>7</sup> <https://www.isdc.unige.ch/integral/science/catalogue>



to  $r \sim 0^\circ$ ) and a low level of the background (linear increase), making the background ratio increase smoothly and  $r_{\text{sep}}$  larger. Indeed, the peak in the distance profile has a e-folding width of  $0.024^\circ$  in the BAT-IBIS catalog cross-match, while it is  $0.082^\circ$  in the BAT-LAT catalog cross-match (Figure 1). With the separation threshold of  $r_{\text{sep}}=0.22^\circ$ , roughly 700 sources were matched. This indicates that we had about 900 sources detected with BAT but not with IBIS (i.e., the *Swift*-BAT catalog has roughly 1600 sources, of which 700 are also detected by *INTEGRAL*), and most of these sources were extragalactic, where the *Swift*-BAT had better sensitivity. On the other hand, there were about 500 sources detected with IBIS but not with BAT, and they were distributed more on the Galactic plane, of which *INTEGRAL* had deeper exposure. Therefore, the IBIS catalog can compensate for the sky region that has not been deeply covered by *Swift*-BAT.

We cross-matched the IBIS catalog and 4FGL-DR2 in the same way as described in Section 3. The spatial match with  $r_{\text{sep}}=0.06^\circ$  resulted in 77 matched point-like sources, including 11 new sources that were not matched in the *Swift*-BAT and *Fermi*-LAT catalog match. Among the 11 sources, 4 were false matches, and 1 was unidentified (NVSS J175948–230944 in 4FGL-DR2 and IGR J17596–2315 in the IBIS catalog). The remaining 6 sources were 3 FSRQs (PKS 1451–375, PKS 1730–13, PKS 1933–400), a bl (MS 1458.8+2249), an agn (PKS 1821–327), and a radio galaxy (M 87). The identification match added two more sources (a radio galaxy (Can B) and an fsrq (PKS 1741–03)). 39 extended LAT sources were also matched, however, including 27 sources overlapped with the *Swift*-BAT catalog in Table 2, 2 false-matched sources, and 6 unidentified sources. This led to 4 firmly matched extended sources: an SNR (IC 433), a PWN (HESS J1825–137), and 2 spp sources (Ken 73 and HESS J1632–478). In summary, in addition to the matched sources between the *Swift*-BAT and *Fermi*-LAT catalogs (Table 1 and Table 2), we found 8 point-like sources and 4 extended sources which were newly and firmly matched between the IBIS catalog and 4FGL-DR2.

Finally, we report on a comparison with *INTEGRAL*-SPI sources. The *INTEGRAL* catalog contains 277 SPI sources in the 20 keV–8 MeV band (with ‘SPI.FLAG’ being 1) in the latest version. 29 SPI sources are matched with 4FGL-DR2 by adopting  $r_{\text{sep}}=0.06^\circ$ , which is determined in the same way presented in Section 3.1. Among them, 26 are included in the BAT-LAT matching, one is a IBIS-LAT matched source, and the remain-

ing two sources are false matches or ambiguous associations.

### 5.1.3. Comparison with 1FLE

Principe et al. (2018) provided the first *Fermi*-LAT low energy catalog (1FLE). This catalog was based on the 8.7-yr *Fermi*-LAT data taken from August 4, 2008 to May 3, 2017 in the energy range of 30–100 MeV. It should be noted that the PSF of even PSF3 events<sup>8</sup> is larger than  $3^\circ$  at  $\leq 100$  MeV, which is comparable with that of COMPTEL,  $3\text{--}5^\circ$ . In the 1FLE catalog, 198 sources were detected at above  $3\sigma$ . Among these 198 sources, 11 sources were not associated with the previous 4-yr *Fermi*-LAT catalog (3FGL; Acero et al. (2015)), 4FGL, and 4FGL-DR2.

A spatial cross-match between the *Swift*-BAT 105-month catalog and 1FLE with  $r_{\text{sep}}=0.25^\circ$ , which is comparable with the positional error of the 1FLE catalog, resulted in 19 matched point-like sources, of which 5 sources (AX J1639.0–4642, Mrk 766, Mrk 841, AX J1639.0–4642, and SWIFT J1521.6+3204) were not included in Table 1. A cross-matching by the source names resulted in 35 sources being matched. For the name-matched sources, the separation of the source coordinate between the *Swift*-BAT catalog and 1FLE was at most  $1.3^\circ$ , which is smaller than the PSF of 1FLE of  $\geq 3^\circ$ . Note that 14 sources are overlapped between the positionally matched sources and the name-matched sources, and thus the total number of point-like sources matched between the *Swift*-BAT catalog and 1FLE is 40. In our cross-matched catalog (Table 1), we show these sources which have counterparts in 1FLE by labelling as ‘1FLE’. Additionally, two extended sources, RX J1713.7–3946 and HESS J1632–478, have counterparts in 1FLE. The BAT-1FLE matched sources have photon indices  $\lesssim 2$  in the energy band of *Swift*-BAT and  $\gtrsim 3$  in the energy band of *Fermi*-LAT except for Mrk 421 with  $\Gamma_{\text{BAT}} > 2$  and  $\Gamma_{\text{Fermi}} > 2$ , NGC 1275 with  $\Gamma_{\text{BAT}} > 2$ , and RX J0115.7+2519 with  $\Gamma_{\text{Fermi}} < 3$ . It should be noted that all the 1FLE sources matched here had associations with sources of 3FGL, and the unidentified 11 1FLE sources were not matched with the BAT sources.

### 5.1.4. Comparison with Maselli et al. 2011

In a previous study, Maselli et al. (2011) performed a catalog cross-match by using the 54-month *Swift*-BAT catalog (2PBC; 1256 sources; a flux sensitivity of  $(0.92\text{--}1.0) \times 10^{-11}$  erg cm<sup>−2</sup> s<sup>−1</sup>; Cusumano et al. (2010)) and

<sup>8</sup> Gamma rays in Pass 8 data are separated into 4 PSF event types, 0, 1, 2, and 3, where PSF0 has the largest PSF and PSF3 has the best.

the 1-yr *Fermi*-LAT catalog (1FGL; 1451 sources; a flux sensitivity of  $10^{-11}$ – $10^{-10}$  erg cm $^{-2}$  s $^{-1}$ ; [Abdo et al. \(2010\)](#)). They reported 62 sources as firmly cross-matched sources which had the same identifications between the two catalogs. Furthermore, 46 sources were positionally matched if the  $Q$  parameter (defined as  $(r_{\text{BAT}} + r_{\text{LAT}})/r_{\text{BL}}$  where  $r_{\text{BAT}}$ ,  $r_{\text{LAT}}$ , and  $r_{\text{BL}}$  are respectively the position uncertainty of a BAT source, that of a LAT source, and the higher value between  $r_{\text{BAT}}$  and  $r_{\text{LAT}}$ ) was set to be  $< 1.0$  (see [Maselli et al. 2011](#), for details). 87 sources in total were matched by the aforementioned positional and identification matching, since 21 sources were overlapped in the two methods. By decreasing the X-ray detection threshold to  $3\sigma$  from  $4.8\sigma$ , the number of the hard X-ray emitting BAT sources in the direction of 1FGL sources increased to 104, which include all the 87 cross-correlated sources.

Among the firmly associated 62 sources in [Maselli et al. \(2011\)](#), 8 were not included in our analysis (Table 1). However, this discrepancy is attributed to the fact that these 8 sources were excluded either in the latest *Swift*-BAT or *Fermi*-LAT catalogs. The following 6 sources are included in 4FGL-DR2, but omitted in the latest BAT catalog probably due to flux time variation: OI +280 in the *Swift*-BAT 54-month catalog (PKS 0748+126 in 1FGL), RX J0948.8+0022 (CGRaBS J0948+0022), RBS 1420 (1ES 1440+122), Ap Lib, PG 1553+113, and PG 0727–11 (PKS 0727–11). ESO 323–77 is in the BAT 105-month catalog, but not included in 4FGL-DR2 ([Maselli et al. \(2011\)](#) also mentioned that this source is a confused LAT source). The remaining one source, 1RXS J033913.4–173553 (PKS 0336–177) had  $Q > 1$  (i.e., spatially unmatched) in [Maselli et al. \(2011\)](#), and thus was not matched in our study. In conclusion, all the firmly matched sources in [Maselli et al. \(2011\)](#) resulted in being matched in this paper, unless the sources were not excluded in the later *Swift*-BAT or *Fermi*-LAT catalogs. The number of the firmly matched sources roughly doubled in this study owing to the developed flux sensitivity of the observations, particularly that of *Fermi*-LAT which was almost one order of magnitude better.

### 5.2. Property of matched sources

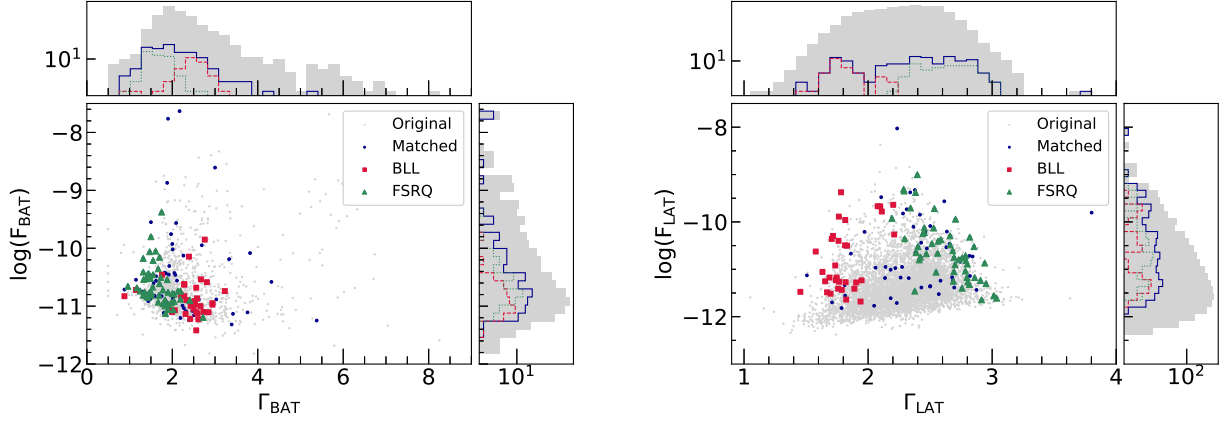
In the following, we compare the photon index, flux, and time variability of the matched and unmatched sources in order to investigate the properties of the matched sources.

Figure 3 shows a correlation between a photon index ( $\Gamma$ ) and flux and their distributions for the matched sources in this catalog and all sources in the original catalog. Here we used the firmly matched point-like sources

(136 in total) with Flag being M or D in Table 1. Even when including the firmly matched extended sources, the following results did not largely change. For the BAT sources (the left panel of Figure 3), the distribution of  $\Gamma$  for the matched sources was slightly shifted to the harder side compared to that of all sources, while the distribution of the flux was shifted to the brighter side. By using Kolmogorov-Smirnov (KS) statistic, we evaluated the difference of the distributions of  $\Gamma$  and the flux between the matched sources and all sources in the original catalog. The  $\Gamma$  distribution showed the value of KS statistic of 0.196 and the p-value of 0.000160, which corresponded to  $3.8\sigma$ , while the flux distribution showed the value of KS statistic of 0.147 and the p-value of 0.00973, which corresponded to  $2.6\sigma$ . Hence, the distributions of  $\Gamma$  and the flux had different properties at the level of  $\sim 3\sigma$ .

For LAT sources (the right panel of Figure 3), the  $\Gamma$  distribution shows an apparent bimodal feature, and the distribution of the flux was clearly shifted to the brighter side, compared to all sources in the original catalog. Similar to the aforementioned results of the BAT sources, we also found that the distributions of  $\Gamma$  and the flux of the matched sources were different from those of the original catalog. The KS statistics and the corresponding p-value were respectively 0.192 and 0.000140 ( $3.8\sigma$ ) in the  $\Gamma$  distribution, while they were respectively 0.427 and  $1.49 \times 10^{-21}$  (over  $5\sigma$ ) in the flux distribution.

The difference in the  $\Gamma$  and flux properties can be explained as follows. Among the matched point sources, the two largest populations were FSRQs (50 sources) and BLLs (33 sources). These two classes of blazars might be part of the blazar sequence, with the synchrotron and high-energy peak at different energy bands: in the energy range of *Swift*-BAT and *Fermi*-LAT, FSRQs have concave-structure (i.e., hard in X-ray and soft in gamma-ray), while BLLs have convex-structure (i.e., soft in X-ray and hard in gamma-ray). Indeed, the double-peak feature in the  $\Gamma$  distribution was ascribed to the  $\Gamma$  distributions of the FSRQs and BLLs (Figure 3). It also should be noted that the fraction of the FSRQs in the matched sources was notably larger than that of the original catalog (Figure 2), making the  $\Gamma$  distributions modified. The difference in the flux distributions can arise from the difference in flux sensitivity between *Swift*-BAT and *Fermi*-LAT. Particularly the flux distribution of the Fermi sources showed the remarkable distinction between the matched and all sources. The better sensitivity of *Fermi*-LAT resulted in the difference in the flux distributions, recalling that the flux



**Figure 3.** Correlation between  $\Gamma$  and flux and their distributions of the *Swift*-BAT (left) and *Fermi*-LAT (right) sources. The grey and blue points are distributions of all the sources in the catalog and the spatially matched sources, respectively. The distributions of the matched BLLs and FSRQs are shown in red and green, respectively. The histograms are shown in logarithmic scale. The figure includes the 136 sources which are firmly matched by the coordinates and the identifications, with the Flag being M or D.

sensitivity of *Swift*-BAT and *Fermi*-LAT are respectively  $8 \times 10^{-12} \text{ erg cm}^{-2} \text{ s}^{-1}$  and  $\sim 1 \times 10^{-12} \text{ erg cm}^{-2} \text{ s}^{-1}$ .

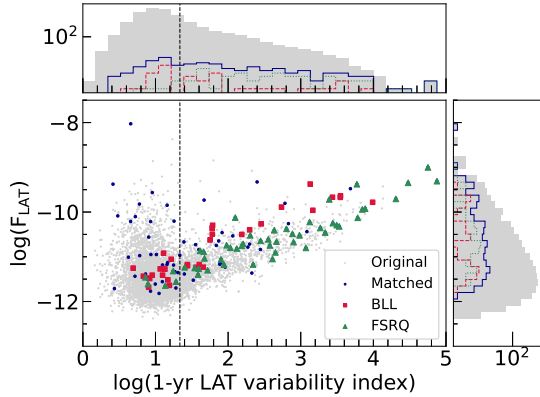


**Figure 4.** Same as Figure 3 for correlation between the 1-yr variability index and flux of the *Fermi*-LAT sources. The 1-yr variability index of  $>21.67$ , shown by the vertical dashed line, means  $<1\%$  chance of a steady source.

We also investigated property of time variation of the matched sources. 4FGL-DR2 provides us with ‘Variability Index’, which is defined as a sum of  $2 \times \text{Log}(\text{Likelihood})$  difference between flux of each time and the averaged one. For the 10-yr lightcurve with 1-yr bin, the variability index of  $> 21.67$  indicates a  $< 1\%$  chance for a steady source. It should be noted that lightcurves with 1-yr bin and 2-month bin were available in 4FGL (the previous 8-yr *Fermi*-LAT catalog), while only lightcurves with 1-yr bin were provided in 4FGL-DR2. We made sure that the variability indices of the 1-yr and 2-month lightcurves were correlated, and

the following results produced by 4FGL-DR2 were consistent with when using the corresponding variability index of the 2-month lightcurves in 4FGL.

Figure 4 shows a correlation between the variability index and the flux and their distributions of the matched sources in our catalog and the all sources in the *Fermi*-LAT catalog. There seem to be two groups in the scatter plot in Figure 4: the correlated variability index and flux (i.e., the time variation can be easily detected for the brighter source) and the smaller variability index with the widely ranged flux (i.e., possible steady source). The distribution of the variability index of the matched sources was also different from that of the original catalog, inferred from the KS statistics and p-value of 0.414 and  $3.29 \times 10^{-20}$  ( $> 5\sigma$ ), respectively.

Our matched sources turned out to be more variable than the sources in the original catalog. This discrepancy arised from the fact that the matched sources mainly consisted of FSRQs and BLLs (Figure 2), which tended to have large variability indices. In the original catalog, 80% of FSRQs are variable with the index of  $> 21.67$ , and 43% of BLLs are so. The difference in the distribution of the variability index could also be attributed to the fact that the brighter sources, correlated to the larger variability index, were more matched in this study.

We present the correlation of the photon indices between the firmly matched *Swift*-BAT and *Fermi*-LAT sources in Figure 5. As seen in Figure 3, the  $\Gamma_{\text{BAT}}-\Gamma_{\text{LAT}}$  diagram also confirmed two distinct populations, BLLs and FSRQs. The right panel of Figure 5 shows the correlation of the flux of the firmly matched *Swift*-BAT and *Fermi*-LAT sources. In the hard X-ray band, the

flux of the matched BLLs tends to be smaller than that of the matched FSRQs.

To summarize, Figure 3 and Figure 4 suggest that our matched sources can be characterized by the double peak in the  $\Gamma$  distribution, the higher flux, and the larger variability index, compared to the all sources in the original catalogs. This difference would be reflected by the features of the two main populations, FSRQs and BLLs.

### 5.3. Unidentified point-like sources

Here we report on the unidentified point-like sources found in our analysis and discuss possible associations. The unidentified source is defined as the positionally matched source with its source type being unclear either in the *Swift*-BAT or *Fermi*-LAT catalogs. Figure 6 shows SEDs of the 9 unidentified sources. Each source is briefly described in the following.

1. No. 58 in Table 1: SWIFT J1254.9+1165 (U3<sup>9</sup>) in the BAT catalog was matched with ON 187 (fsrq) in 4FGL-DR2. They are possibly associated, inferred from the FSRQ-like SED and the small separation of  $0.006^\circ$ .
2. No. 65: SWIFT J0949.1+4057 (confused source) in the BAT catalog was matched with 4C +40.24 (fsrq) in 4FGL-DR2. This association needs more investigation to be confirmed, particularly in the hard X-ray energy range that was uncertain due to the large errors. Deeper observations would give us a clue for such a faint source.
3. No. 75: PMN J0145-2733 (Unknown AGN) in the BAT catalog was matched with PKS 0142-278 (fsrq) in 4FGL-DR2. This could be likely an association, inferred from the FSRQ-like SED. However, more X-ray observations would be necessary to precisely measure the upturn-like feature seen at  $\sim 70$  keV in order to determine its origin and the association with the GeV gamma-ray radiation.
4. No. 130: GX 340+0 (LMXB) in the BAT catalog was matched with 4U 1642-45 (unk) in 4FGL-DR2. The association between these two sources is promising, since they have the same identification. The GeV emission with *Fermi*-LAT, however, is unknown due to being located in a complex TeV gamma-ray emitting region, HESS

J1648–458 (see, e.g., Abramowski et al. 2012). Beside the accreting neutron star 4U 1642–45, HESS J1648–458 contained PSR J1648–4611 and a star cluster Westerlund 1. 4U 1642–45 was unlikely responsible for the TeV gamma rays, inferred from the spatial extent and time variation. They argued that a single source scenario would favor the hadronic gamma-ray radiation produced by collisions of cosmic rays from Westerlund 1 with the interstellar medium (ISM).

5. No. 131: SAX J1808.4–3658 (LMXB) in the BAT catalog was matched with SWIFT J1808.5–3655 (unknown) in 4FGL-DR2. Note that the counterpart of the *Fermi* source is not a firm association (i.e., SWIFT J1808.5–3655 was labeled with ‘AS-SOC2’). This association—the gamma-ray emission from the LMXB—was previously reported and discussed in de Oña Wilhelmi et al. (2016).
6. No. 132: XTE J1652–453 (LMXB) in the BAT catalog was matched with SWIFT J1652.3–4520 (unknown) in 4FGL-DR2. Note that the counterpart of the *Fermi* source is not a firm association (i.e., SWIFT J1652.3–4520 was labeled with ‘AS-SOC2’). They might be associated as the former case of SAX J1808.4–3658, although further investigation is needed to confirm the association.
7. No. 154–156: CGCG 147–020 (Sy2; No. 154), 2MASX J14080674–3023537 (Sy1.9; No. 155), and XTE J1817–330 (LMXB; No. 156) are the matched *Swift*-BAT sources, and they are unknown sources in 4FGL-DR2. These were faint, and thus the position uncertainty was large both in the BAT and LAT observations. The dedicated deeper observations are necessary for them to unveil the association and the nature.

We conducted a time variation analysis of the unidentified point-like sources using 1-month lightcurves of the *Swift*-BAT catalog and 2-month lightcurves of 4FGL (the 8-yr *Fermi*-LAT catalog). No significant correlation between the hard X-ray and GeV gamma-ray radiation in the 2-month scale was found in any unidentified source, probably because of the poor statistics. In the case of the binary system, timing analyses folded by the orbital period are necessary to track the variability correlation. This is beyond the scope of this paper and will be performed in the future publication.

<sup>9</sup> ‘U3’ indicates unknown sources without soft X-ray counterparts in the *Swift*-BAT 105-month catalog.



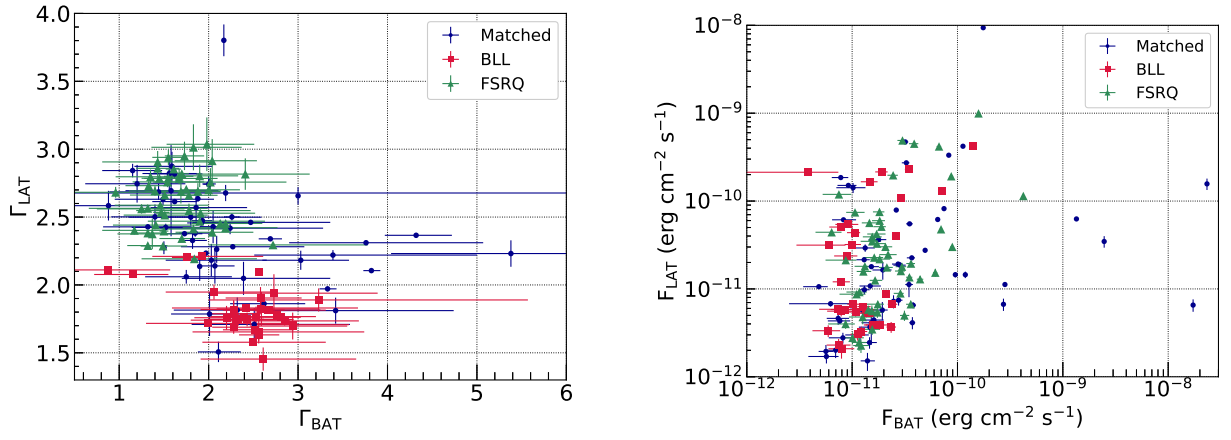


**Figure 5.** Scatter plots of the  $\Gamma$  (left) and flux (right) of the firmly matched *Swift*-BAT and *Fermi*-LAT sources. The red and green respectively show those of BLLs and FSRQs, and the blue indicates those of the rest sources.

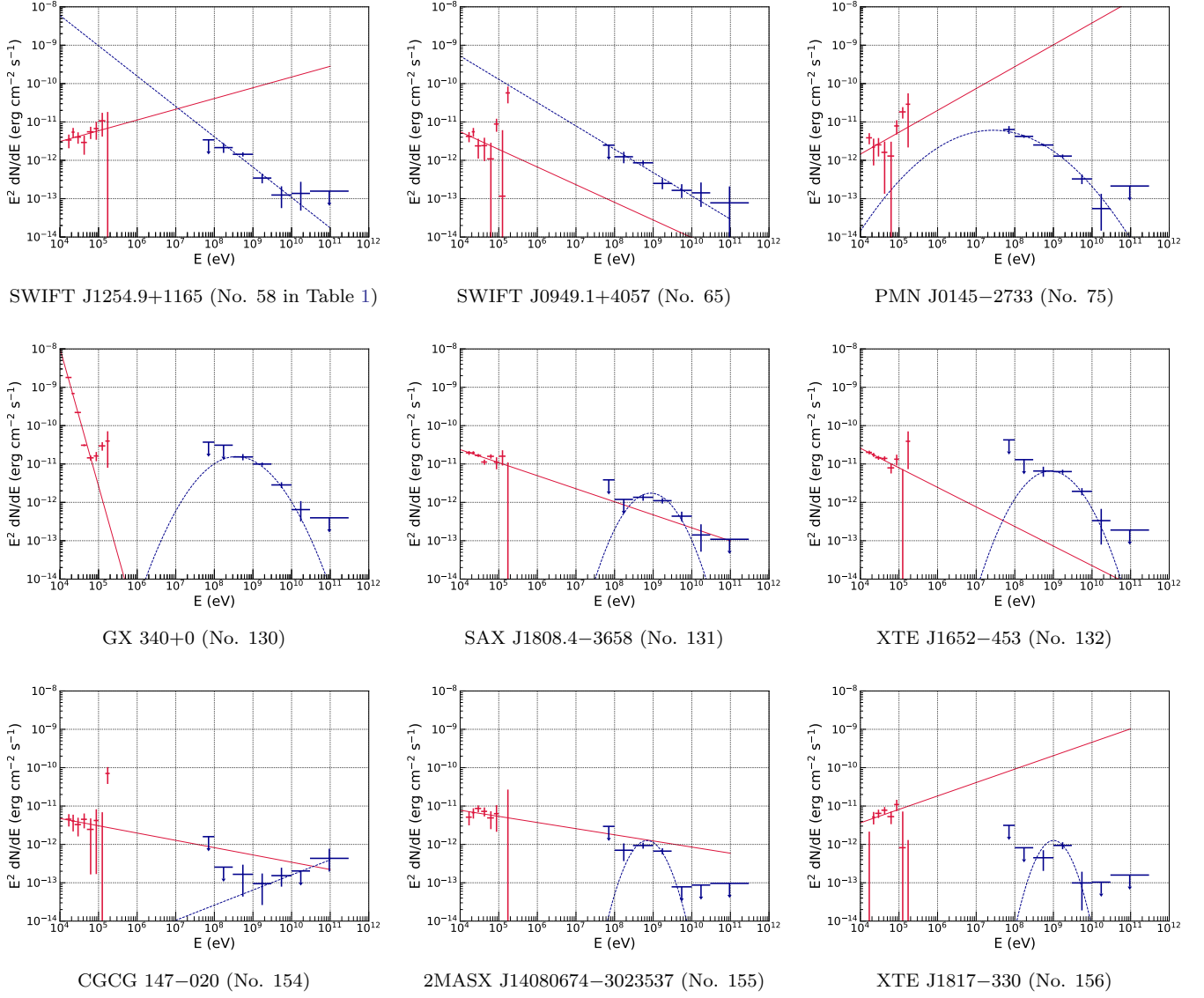


**Figure 6.** SEDs of the unidentified point-like sources in the *Swift*-BAT (14–195 keV) and *Fermi*-LAT (50 MeV–300 GeV) energy bands, shown in red and blue, respectively. The red solid and blue dashed lines indicate the model spectrum taken from the *Swift*-BAT and *Fermi*-LAT catalogs, respectively.

#### 5.4. Unidentified extended sources

We briefly describe the current status of the unidentified and extended sources in our study. Their SEDs are illustrated in Figure 7.

1. No. 17 in Table 2: Sim 147 (SNR) was spatially matched with SWIFT J053457.91+282837.9 (U2<sup>10</sup>) in the *Swift*-BAT catalog. Sim 147 is a middle-aged SNR, including a known PSR-PWN association inside its GeV gamma-ray extent of  $1.5^\circ$  (Katsuta et al. 2012). The matched source, SWIFT J053457.91+282837.9, was revealed to be a possible intermediate polar (i.e., a cataclysmic variable binary star system) by a periodic analysis of optical observations (Halpern 2018). Therefore we suggest that these two sources are not associated and are false-matched. This would also be supported by the fact that the BAT source is located near the edge of the gamma-ray emission, and there exists the aforementioned PSR-PWN association close to the center of the SNR.
2. No. 29: FGES J1036.3–5833 (unidentified) hosts inside the extent Eta Carina (XRB), 4U 1036–56 (HMXB), and 2MASS J10445192–6025115 (star). This gamma-ray emission is largely extended with  $\sim 2.5^\circ$  in radius, and is remarkably variable in the 1-yr scale with the variability index of  $\sim 75$ . The time variation could result from a variable source inside the gamma-ray extent (i.e., Eta Carina or 4U 1036–56).
3. No. 30: FGES J1409.1–6121 (unidentified) has spatial coincidences with SWIFT J1408.2–6113 (CV), [CG2001] G311.45–0.13 (U2), and MAXI J1409–619 (Pulsar). The gamma-ray extent is  $\sim 0.73^\circ$ . The gamma-ray emission might be associated with [CG2001] G311.45–0.13, which could be a possible counterpart of a radio SNR G12.4–0.4 (Doherty et al. 2003). However, the hard spectrum in the *Swift*-BAT energy regime ( $\Gamma \sim 2$ ) is not likely of origin of the X-ray radiation from the remnant. An alternative is MAXI J1409–619, a pulsar, which is located in the vicinity of SNR G12.4–0.4. Further investigation would be necessary to confirm the association.
4. No. 31: HESS J1808–204 (unidentified) was spatially matched with SGR 1806–20 (a pulsar, more like a magnetar) in the *Swift*-BAT catalog. Yeung

(2016) reported the possible association between the gamma-ray radiation with *Fermi*-LAT and the magnetar, and later the origin (i.e., the gamma-ray emission powered by magnetic dissipation from SGR 1806–20) was discussed in H.E.S.S. Collaboration et al. (2018). These studies, however, could not reach to a robust conclusion due to other plausible scenarios to account for the gamma-ray radiation.

#### 5.5. Future prospect

Over 20 years ago, COMPTEL confirmed 25 steady MeV gamma-ray emitting sources based on the observational data with the flux sensitivity of  $\sim 10^{-10}$  erg cm<sup>-2</sup> s<sup>-1</sup> (Schönfelder et al. 2000). In the last decade, the sensitivity of the detectors in the neighboring energy bands (i.e., the hard X-ray and GeV gamma ray) has improved to  $< 10^{-11}$  erg cm<sup>-2</sup> s<sup>-1</sup>. This work reports 151 sources firmly matched between the latest *Swift*-BAT and *Fermi*-LAT catalogs. We present these cross-matched sources in the all-sky map in Figure 8. The matched catalog (Table 1 and Table 2) contains promising objects that are bright in the MeV energy range and are detectable with future instruments with a sensitivity being over one order of magnitude better than COMPTEL. This catalog would be a helpful resource when devising a strategy for the ongoing projects of the MeV observation, such as *e-ASTROGAM* (De Angelis et al. 2018), *AMEGO* (McEnery et al. 2019), *COSI* (Tomsick et al. 2019), and *GRAMS* (Aramaki et al. 2020). The cross-matched sources, combined with a simulation of diffuse emission, can be useful to predict the all sky image in the MeV energy channel. This will be presented in a future publication.

<sup>10</sup> U2 indicates a source of which its soft X-ray emission is detected from archival X-ray observation with S/N greater than 3.

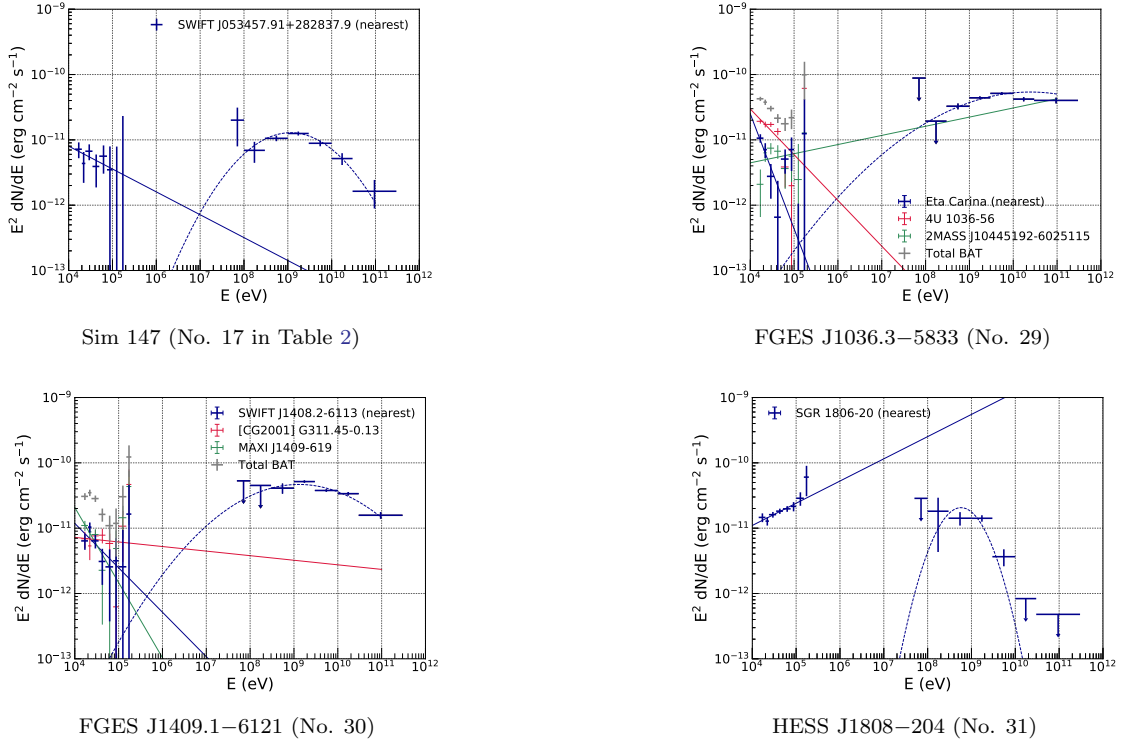


**Figure 7.** SEDs of unidentified extended sources. The blue solid and dashed lines indicate the model spectra provided in the *Swift*-BAT and *Fermi*-LAT catalogs, respectively. For FGES J1036.3–5833 and FGES J1409.1–6121, SEDs of all BAT counterparts and the total flux are also shown.

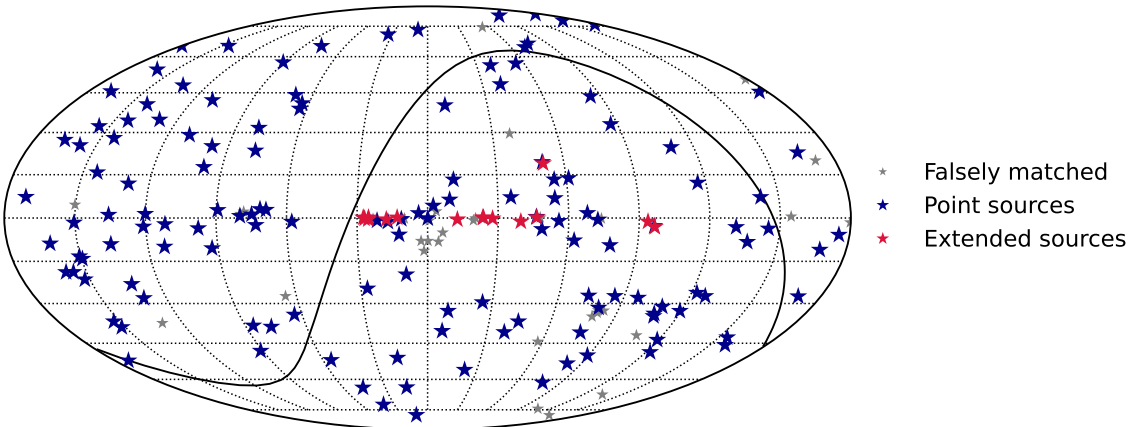


**Figure 8.** The cross-matched sources shown on the galactic coordinate. The firmly matched point sources and extended sources are shown in blue and red, respectively, while the false matches are shown in grey. The solid line indicates the declination of  $0^\circ$ .



## 6. CONCLUSIONS

We performed a cross-match between the *Swift*-BAT 105-month catalog and the 4FGL-DR2 catalog. We confirmed (1) 132 sources (115 firmly matched sources) by the spatial cross-match with the separation threshold of  $r_{\text{sep}}=0.08^\circ$ , (2) 31 sources (15 firmly matched sources) by the spatial cross-match for extended sources, and (3) 24 sources (21 firmly matched sources) by the identification match. The firmly matched sources (151 in total) predominantly consisted of blazars. Particularly, the proportion of FSRQs in the matched catalog was over twice as large as that of the 4FGL-DR2. We found that most of COMPTEL sources were included in this study, and the cross-match with *INTEGRAL*-IBIS catalog could add 8 point-like and 4 extended sources. Compared to the original catalogs, the distributions of physical parameters of the matched

sources were characterized by the bimodal feature in the  $\Gamma$  distribution, a higher flux, and larger variability index, resulting from the different source fractions.

## ACKNOWLEDGMENTS

We thank the anonymous referee for the fruitful comments and advise. This work made use of data from the *Swift* and *Fermi* observatories. N.T. acknowledges RIKEN iTHEMS Program. H.Y. is supported by the Japan Society for the Promotion of Science (JSPS) KAKENHI grant No. 20K22355, Y.I. is supported by JSPS KAKENHI grant Nos. JP16K13813, JP18H05458, and JP19K14772, and H.O. is supported by JSPS KAKENHI grant Nos. 19H05185 and 19H01906.

*Facilities:* *Swift*-BAT, *Fermi*-LAT

## REFERENCES

- Abdo, A. A., Ackermann, M., Ajello, M., et al. 2010, The Astrophysical Journal Supplement Series, 188, 405
- Abdollahi, S., Acero, F., Ackermann, M., et al. 2020, The Astrophysical Journal Supplement Series, 247, 33
- Abramowski, A., Acero, F., Aharonian, F., et al. 2012, Astronomy & Astrophysics, 537, A114
- Acero, F., Ackermann, M., Ajello, M., et al. 2015, The Astrophysical Journal Supplement Series, 218, 23
- Ackermann, M., Ajello, M., Allafort, A., et al. 2012, The Astrophysical Journal, 755, 164
- Aramaki, T., Adrian, P. O. H., Karagiorgi, G., & Odaka, H. 2020, Astroparticle Physics, 114, 107
- Araya, M., & Herrera, C. 2021, Monthly Notices of the Royal Astronomical Society, doi:10.1093/mnras/stab101
- Atwood, W. B., Abdo, A. A., Ackermann, M., et al. 2009, The Astrophysical Journal, 697, 1071
- Ballet, J., Burnett, T. H., Digel, S. W., & Lott, B. 2020, arXiv:2005.11208 [astro-ph], arXiv:2005.11208
- Barthelmy, S. D., Barbier, L. M., Cummings, J. R., et al. 2005, Space Science Reviews, 120, 143
- Bird, A. J., Bazzano, A., Malizia, A., et al. 2016, The Astrophysical Journal Supplement Series, 223, 15
- Bloemen, H., Bennett, K., Blom, J. J., et al. 1995, Astronomy and Astrophysics, 293
- Cusumano, G., Parola, V. L., Segreto, A., et al. 2010, Astronomy & Astrophysics, 524, A64
- De Angelis, A., Tatischeff, V., Grenier, I. A., et al. 2018, Journal of High Energy Astrophysics, 19, 1
- de Martino, D., Belloni, T., Falanga, M., et al. 2013, Astronomy & Astrophysics, 550, A89
- de Oña Wilhelmi, E., Papitto, A., Li, J., et al. 2016, Monthly Notices of the Royal Astronomical Society, 456, 2647
- Doherty, M., Johnston, S., Green, A. J., et al. 2003, Monthly Notices of the Royal Astronomical Society, 339, 1048
- Ferrand, G., & Safi-Harb, S. 2012, Advances in Space Research, 49, 1313
- Gehrels, N., Chincarini, G., Giommi, P., et al. 2004, The Astrophysical Journal, 611, 1005
- H. E. S. S. Collaboration, Abdalla, H., Abramowski, A., et al. 2018, 612, A1
- Halpern, J. P. 2018, The Astronomical Journal, 24
- H.E.S.S. Collaboration, Abdalla, H., Abramowski, A., et al. 2018, Astronomy & Astrophysics, 612, A11
- Hitomi Collaboration, Aharonian, F., Akamatsu, H., et al. 2018, Publications of the Astronomical Society of Japan, 70, doi:10.1093/pasj/psy027
- Inoue, Y., Khangulyan, D., & Doi, A. 2020, The Astrophysical Journal, 891, L33
- Inoue, Y., Khangulyan, D., Inoue, S., & Doi, A. 2019, The Astrophysical Journal, 880, 40
- Itoh, R., Utsumi, Y., Inoue, Y., et al. 2020, arXiv e-prints, 2008, arXiv:2008.00038
- Kataoka, J., Stawarz, \., Takahashi, Y., et al. 2011, The Astrophysical Journal, 740, 29
- Katsuta, J., Uchiyama, Y., Tanaka, T., et al. 2012, The Astrophysical Journal, 752, 135
- Maselli, A., Cusumano, G., Massaro, E., et al. 2011, Astronomy and Astrophysics, 531, A153

- McEnery, J., Barrio, J. A., Agudo, I., et al. 2019, arXiv:1907.07558 [astro-ph], arXiv:1907.07558
- Oh, K., Koss, M., Markwardt, C. B., et al. 2018, The Astrophysical Journal Supplement Series, 235, 4
- Paliya, V. S., Koss, M., Trakhtenbrot, B., et al. 2019, The Astrophysical Journal, 881, 154
- Principe, G., Malyshev, D., Ballet, J., & Funk, S. 2018, Astronomy & Astrophysics, 618, A22
- Schoenfelder, V., Aarts, H., Bennett, K., et al. 1993, The Astrophysical Journal Supplement Series, 86, 657
- Schönfelder, V., Bennett, K., Blom, J. J., et al. 2000, Astronomy and Astrophysics Supplement Series, 143, 145
- Takahashi, T., Uchiyama, Y., & Stawarz, L. 2013, Astroparticle Physics, 43, 142
- Toda, K., Fukazawa, Y., & Inoue, Y. 2020, The Astrophysical Journal, 896, 172
- Tomsick, J. A., Zoglauer, A., Sleator, C., et al. 2019, arXiv:1908.04334 [astro-ph], arXiv:1908.04334
- Ubertini, P., Lebrun, F., Cocco, G. D., et al. 2003, Astronomy & Astrophysics, 411, L131
- Winkler, C., Cocco, G. D., Gehrels, N., et al. 2003, Astronomy & Astrophysics, 411, L1
- Yeung, P. K. H. 2016, The Astrophysical Journal, 8

Table 1. Cross-matched point-like sources

No.	<i>Swift</i> -BAT name	Type	<i>Fermi</i> -LAT name	Type	Sep. (deg)	Flag	1FLE	BAT coord. ( $\alpha_{J2000}, \delta_{J2000}$ )	$\Gamma_{\text{BAT}}$	$\Gamma_{\text{LAT}}$	$F_{\text{BAT}}$	$F_{\text{LAT}}$	VarIndex
1	[HB89] 0537-441	Beamed AGN	PKS 0537-441	BLL	0.063	M	1	(84.63, -44.12)	0.88	2.11	1.5	17	9.8e+03
2	[HB89] 0716+714	Beamed AGN	S5 0716+71	BLL	0.01	M	1	(110.5, 71.33)	1.15	2.08	1.9	21	2.7e+03
3	Mrk 421	Beamed AGN	Mkn 421	BLL	0.014	M	1	(166.1, 38.21)	2.76	1.78	14	42	1.3e+03
4	Mrk 501	Beamed AGN	Mkn 501	BLL	0.001	M	0	(253.5, 39.76)	2.39	1.76	7.2	13	5.4e+02
5	BL Lac	Beamed AGN	BL Lac	BLL	0.018	M	1	(330.7, 42.27)	1.76	2.2	3.5	23	3.5e+03
6	1ES 0033+595	Beamed AGN	1ES 0033+595	bl	0.008	M	0	(8.989, 59.84)	2.81	1.76	2.6	4	2e+02
7	2MASX J01155048+2515369	Sy1	RX J0115.7+2519	bl	0.018	A	0	(18.97, 25.33)	1.97	1.92	1.1	2	3.1e+02
8	SHBL J012308.7+342049	Beamed AGN	1ES 0120+340	bl	0.021	M	0	(20.78, 34.37)	2.94	1.7	1.1	0.3	15
9	B3 0133+388	Beamed AGN	B3 0133+388	bl	0.052	M	0	(24.13, 39.05)	1.99	1.72	0.79	5.1	61
10	RBS 259	Beamed AGN	1RXS J015658.6-530208	bl	0.062	M	0	(29.13, -53.04)	2.31	1.74	0.73	0.59	45
11	2MASX J02141794+5144520	Beamed AGN	TXS 0210+515	bl	0.03	M	0	(33.55, 51.77)	2.58	1.9	1.4	0.53	13
12	QSO B0229+200	Beamed AGN	1ES 0229+200	bl	0.036	M	0	(38.19, 20.29)	2.28	1.79	2.3	0.37	6.8
13	ESO 416-G002	Sy1.9	PHL 1389	bl	0.068	A	0	(38.83, -29.63)	1.67	2.03	2.1	0.17	14
14	BZB J0244-5819	Beamed AGN	RBS 0351	bl	0.031	M	0	(41.19, -58.3)	2.43	1.75	1	0.67	40
15	QSO B0347-121	Beamed AGN	1ES 0347-121	bl	0.018	M	0	(57.37, -11.98)	2.2	1.76	1.6	0.39	13
16	PKS 0352-686	Beamed AGN	PKS 0352-686	bl	0.004	M	0	(58.28, -68.53)	2.52	1.67	1.2	0.33	8.3
17	PKS 0426-380	Beamed AGN	PKS 0426-380	bl	0.059	M	0	(67.14, -37.89)	2.56	2.1	0.38	21	3.5e+03
18	PKS 0548-322	Beamed AGN	PKS 0548-322	bl	0.054	M	0	(87.69, -32.27)	3.23	1.89	1.8	0.39	9
19	PMN J0640-1253	Beamed AGN	TXS 0637-128	bl	0.056	M	0	(100.1, -12.87)	2.56	1.65	0.79	0.56	4.9
20	2MASX J07103005+5908202	Beamed AGN	1H 0658+595	bl	0.008	M	0	(107.6, 59.14)	2.28	1.69	2.4	0.67	27
21	2MASS J09303759+4950256	Beamed AGN	1ES 0927+500	bl	0.069	M	0	(142.5, 49.88)	2.59	1.82	0.74	0.23	16
22	2MASS J09343014-1721215	Beamed AGN	RXC J0934.4-1721	bl	0.039	M	0	(143.6, -17.34)	2.73	1.94	0.79	0.21	8
23	2MASX J10311847+5053358	Beamed AGN	1ES 1028+511	bl	0.02	M	0	(157.9, 50.9)	2.85	1.74	0.78	1.2	13
24	2MASX J11033765-2329307	Beamed AGN	1ES 1101-232	bl	0.045	M	0	(165.9, -23.47)	2.53	1.77	1.1	0.55	13
25	2MASX J11363009+6737042	Beamed AGN	RX J1136.5+6737	bl	0.033	M	0	(174.1, 67.64)	2.33	1.75	1.3	0.63	28
26	FBQS J1221+3010	Beamed AGN	PG 1218+304	bl	0.008	M	0	(185.3, 30.16)	2.94	1.71	1.1	4.4	60
27	[HB89] 1415+259	Beamed AGN	1E 1415.6+2557	bl	0.041	M	0	(214.4, 25.72)	2.61	1.45	0.59	0.33	8.1
28	1ES 1426+428	Beamed AGN	H 1426+428	bl	0.027	M	0	(217.1, 42.66)	2.56	1.63	2.1	0.88	16
29	[HB89] 1803+784	Beamed AGN	S5 1803+784	bl	0.057	M	1	(269.9, 78.47)	1.93	2.21	0.91	5.4	2.8e+02
30	QSO B1959+650	Beamed AGN	1ES 1959+650	bl	0.019	M	0	(300, 65.16)	2.67	1.82	2.9	11	1.5e+03
31	2MASX J23470479+5142179	Beamed AGN	1ES 2344+514	bl	0.005	M	0	(356.8, 51.69)	2.66	1.81	1	3.2	60
32	H 2356-309	Beamed AGN	H 2356-309	bl	0.058	M	0	(359.8, -30.58)	2.28	1.82	1.5	0.53	12

Table 1 continued

Table 1 (*continued*)

No.	<i>Swift</i> -BAT name	Type	<i>Fermi</i> -LAT name	Type	Sep. (deg)	Flag	1FLE	BAT coord. ( $\alpha_{J2000}, \delta_{J2000}$ )	$\Gamma_{\text{BAT}}$	$\Gamma_{\text{LAT}}$	$F_{\text{BAT}}$	$F_{\text{LAT}}$	VarIndex
33	3C 454.3	Beamed AGN	3C 454.3	FSRQ	0.011	M	1	(343.5, 16.15)	1.5	2.4	16	1e+02	5.6e+04
34	[HB89] 2230+114	Beamed AGN	CTA 102	FSRQ	0.031	M	1	(338.2, 11.71)	1.49	2.29	3	49	7.5e+04
35	PKS 2227-088	Beamed AGN	PKS 2227-08	FSRQ	0.072	M	1	(337.5, -8.492)	1.46	2.59	1.7	4.2	6.4e+02
36	[HB89] 2142-758	Beamed AGN	PKS 2142-75	FSRQ	0.074	M	1	(327.1, -75.58)	1.41	2.44	1.5	5.6	2.8e+03
37	QSO B2013+370	Beamed AGN	MG2 J201534+3710	FSRQ	0.036	M	0	(303.9, 37.21)	2.13	2.45	1.8	7.5	1.3e+02
38	PKS 1830-21	Beamed AGN	PKS 1830-211	FSRQ	0.017	M	1	(278.4, -21.07)	1.47	2.53	8.7	19	2.5e+03
39	3C 345	Beamed AGN	3C 345	FSRQ	0.026	M	0	(250.8, 39.81)	1.17	2.4	2.1	3	2e+02
40	PKS 1622-29	Beamed AGN	PKS B1622-297	FSRQ	0.034	M	1	(246.6, -29.86)	1.32	2.56	1.6	3.9	4.3e+02
41	PKS 1510-08	Beamed AGN	PKS 1510-089	FSRQ	0.025	M	1	(228.2, -9.081)	1.32	2.38	6.7	42	5.9e+03
42	3C 279	Beamed AGN	3C 279	FSRQ	0.015	M	1	(194.1, -5.799)	1.32	2.29	3.9	45	3e+04
43	3C 273	Beamed AGN	3C 273	FSRQ	0.009	M	1	(187.3, 2.047)	1.75	2.7	42	11	7e+03
44	PG 1222+216	Beamed AGN	4C +21.35	FSRQ	0.021	M	1	(186.2, 21.4)	1.7	2.34	2.5	20	2e+04
45	4C +49.22	Beamed AGN	4C +49.22	FSRQ	0.017	M	1	(178.3, 49.5)	1.83	2.41	1.3	1.6	1.2e+03
46	[HB89] 0836+710	Beamed AGN	4C +71.07	FSRQ	0.004	M	1	(130.3, 70.89)	1.7	2.82	7	4.8	3.4e+03
47	PMN J0641-0320	Beamed AGN	PMN J0641-0320	FSRQ	0.046	M	0	(100.5, -3.362)	0.96	2.68	2.2	2.5	3.6e+02
48	PKS 0528+134	Beamed AGN	PKS 0528+134	FSRQ	0.032	M	0	(82.74, 13.57)	1.25	2.56	1.8	2.2	4.6e+02
49	PKS 0402-362	Beamed AGN	PKS 0402-362	FSRQ	0.017	M	1	(60.97, -36.07)	1.91	2.53	1.1	7.4	6.1e+03
50	PKS 2325+093	Beamed AGN	PKS 2325+093	fsrq	0.012	M	1	(351.9, 9.663)	1.4	2.69	3	1.8	3.7e+02
51	87GB 215950.2+503417	Beamed AGN	NRAO 676	fsrq	0.016	M	1	(330.4, 50.82)	1.78	2.66	1.9	5.1	3.1e+03
52	PKS 2149-306	Beamed AGN	PKS 2149-306	fsrq	0.015	M	1	(328, -30.46)	1.61	2.85	8.9	3	9.6e+02
53	[HB89] 1921-293	Beamed AGN	PKS B1921-293	fsrq	0.063	M	0	(291.2, -29.18)	2.04	2.39	1.6	2.3	2.8e+02
54	2MASS J16561677-3302127	Beamed AGN	2MASS J16561677-3302127	fsrq	0.024	M	0	(254.1, -33.04)	1.55	2.79	6.2	1.5	1.3e+02
55	[HB89] 1354+195	Beamed AGN	4C +19.44	fsrq	0.079	M	0	(209.3, 19.29)	2.02	2.76	0.87	0.4	39
56	[HB89] 1334-127	Beamed AGN	PKS 1335-127	fsrq	0.013	M	0	(204.4, -12.95)	2.19	2.42	1.3	1.8	95
57	PKS 1329-049	Beamed AGN	PKS 1329-049	fsrq	0.032	M	1	(203, -5.153)	1.51	2.51	1.5	3.5	2.2e+03
58	SWIFT J1254.9+1165	U3	ON 187	fsrq	0.006	U	0	(193.7, 11.65)	1.72	2.79	1.3	0.52	28
59	4C +04.42	Beamed AGN	4C +04.42	fsrq	0.047	M	0	(185.6, 4.219)	1.45	2.79	3.6	1.9	1.6e+02
60	FBQS J1159+2914	Beamed AGN	Ton 599	fsrq	0.045	M	1	(179.9, 29.23)	1.84	2.19	0.75	12	7.7e+03
61	7C 1150+3324	Beamed AGN	B2 1150+33A	fsrq	0.053	M	0	(178.2, 33.09)	1.83	3.01	1	0.28	19
62	PKS 1143-696	Beamed AGN	PKS 1143-696	fsrq	0.077	M	0	(176.5, -69.9)	1.69	2.69	1.5	0.56	35
63	PKS 1127-14	Beamed AGN	PKS 1127-14	fsrq	0.065	M	0	(172.5, -14.8)	1.88	2.69	2.9	0.89	4.1e+02
64	[HB89] 1039+811	Beamed AGN	S5 1039+81	fsrq	0.022	M	0	(161.2, 80.92)	1.67	2.78	1.2	0.92	47
65	SWIFT J0949.1+4057	confused source	4C +40.24	fsrq	0.063	U	0	(147.3, 40.57)	2.46	2.61	0.73	0.31	32
66	CGRBS J0805+6144	Beamed AGN	TXS 0800+618	fsrq	0.048	M	0	(121.3, 61.75)	1.35	2.8	1.8	0.67	2.2e+02

Table 1 (*continued*)



Table 1 (*continued*)

No.	<i>Swift</i> -BAT name	Type	<i>Fermi</i> -LAT name	Type	Sep. (deg)	Flag	1FLE	BAT coord. ( $\alpha_{J2000}, \delta_{J2000}$ )	$\Gamma_{\text{BAT}}$	$\Gamma_{\text{LAT}}$	$F_{\text{BAT}}$	$F_{\text{LAT}}$	VarIndex
67	B2 0743+25	Beamed AGN	B2 0743+25	fsrq	0.042	M	0	(116.6, 25.81)	1.43	2.86	3.6	0.67	88
68	PKS 0637-752	Beamed AGN	PKS 0637-75	fsrq	0.038	M	0	(99.02, -75.28)	2.0	2.7	1.7	1.3	4.5e+02
69	[HB89] 0552+398	Beamed AGN	B2 0552+39A	fsrq	0.02	M	0	(88.9, 39.81)	1.54	2.76	2.1	1.8	1.5e+02
70	[HB89] 0537-286	Beamed AGN	PKS 0537-286	fsrq	0.045	M	0	(84.97, -28.7)	1.33	2.73	2.9	1.6	1.1e+02
71	PKS 0524-460	Beamed AGN	PKS 0524-460	fsrq	0.035	M	0	(81.32, -46.01)	1.37	2.38	1.6	0.35	7.3
72	[HB89] 0403-132	Beamed AGN	PKS 0403-13	fsrq	0.061	M	0	(61.36, -13.14)	1.78	2.55	1.1	0.87	80
73	4C +50.11	Beamed AGN	NRAO 150	fsrq	0.017	M	0	(59.9, 50.97)	1.51	2.66	1.7	3.3	7.7e+02
74	[HB89] 0212+735	Beamed AGN	S5 0212+73	fsrq	0.073	M	1	(34.38, 73.81)	1.55	2.94	3.5	1.4	41
75	PMN J0145-2733	Unknown AGN	PKS 0142-278	fsrq	0.042	U	1	(26.21, -27.54)	1.43	2.6	1.1	0.98	8.1e+02
76	ESO 354- G 004	Sy1.9	PMN J0151-3605	bcu	0.007	A	0	(27.87, -36.13)	1.98	2.28	1.1	0.22	8
77	4C +33.06	Beamed AGN	4C +33.06	bcu	0.049	M	0	(46.19, 33.8)	1.86	2.57	1.2	0.3	33
78	PKS 0706-15	Beamed AGN	PKS 0706-15	bcu	0.024	M	0	(107.3, -15.44)	3.42	1.81	0.74	0.46	19
79	PKS 0723-008	Beamed AGN	PKS 0723-008	bcu	0.03	M	0	(111.5, -0.942)	1.75	2.06	1.5	1.1	22
80	2MASX J07332681+5153560	Beamed AGN	NVSS J073326+515355	bcu	0.057	M	0	(113.4, 51.93)	2.32	1.81	0.82	0.28	12
81	IGR J13109-5552	Sy1	PMN J1310-5552	bcu	0.03	D	0	(197.7, -55.91)	1.56	2.82	2.5	0.72	78
82	PMN J1508-4953	Beamed AGN	PMN J1508-4953	bcu	0.013	M	0	(227.2, -49.87)	1.15	2.84	2.9	1.9	36
83	SGR A *	Galactic Center	Galactic Centre	bcu	0.016	D	0	(266.4, -29.01)	2.69	2.34	11	42	2.6
84	PKS 1936-623	Beamed AGN	PKS 1936-623	bcu	0.017	M	1	(295.3, -62.16)	1.32	2.43	1.8	3.6	1.2e+03
85	SWIFT J1943536.21+211822.9	Beamed AGN	MG2 J194359+2118	bcu	0.028	M	0	(296, 21.31)	2.11	1.51	2.8	0.74	15
86	B2 2023+33	Beamed AGN	B2 2023+33	bcu	0.008	M	0	(306.3, 33.68)	1.49	2.63	1.3	2.9	1.2e+02
87	RX J2056.6+4940	Beamed AGN	RGB J2056+496	bcu	0.007	M	0	(314.2, 49.66)	2.62	1.86	1.3	2.1	25
88	RBS 1895	Beamed AGN	RBS 1895	bcu	0.014	M	0	(341.7, -52.12)	2.51	1.71	0.7	0.2	19
89	1RXS J225146.9-320614	Beamed AGN	1RXS J225146.9-320614	bcu	0.044	M	0	(342.9, -32.1)	2.01	1.79	1.4	0.15	11
90	PKS 0521-36	Beamed AGN	PKS 0521-36	AGN	0.018	M	1	(80.76, -36.46)	1.92	2.46	3.5	5.5	6.8e+02
91	Cen A	Beamed AGN	Cen A	RDG	0.012	M	1	(201.4, -43.02)	1.88	2.64	1.3e+02	6.3	18
92	3C 120	Beamed AGN	3C 120	RDG	0.039	M	0	(68.3, 5.356)	2.01	2.74	9.5	1.5	2.8e+02
93	NGC 1275	Beamed AGN	NGC 1275	RDG	0.009	M	1	(49.95, 41.51)	3.82	2.11	8.3	33	4.8e+03
94	PKS 2300-18	Beamed AGN	PKS 2300-18	rdg	0.069	M	0	(345.8, -18.7)	2.03	2.18	1.5	0.25	9.9
95	3C 303	Sy1	3C 303	rdg	0.046	D	0	(220.7, 52.06)	2.39	2.05	0.57	0.17	8.5
96	PICTOR A	Sy2	Pictor A	rdg	0.045	D	0	(79.95, -45.77)	2.05	2.43	3.7	0.41	7.3
97	QSO B0309+411	Beamed AGN	B3 0309+411B	rdg	0.039	M	0	(48.26, 41.29)	1.58	2.69	1.5	0.41	25
98	NGC 4945	Sy2	NGC 4945	sbgr	0.003	D	0	(196.4, -49.47)	1.5	2.27	28	1.1	10
99	M 82	Starburst galaxy	M 82	sbgr	0.029	M	0	(148.9, 69.64)	3.39	2.22	0.48	1.1	6.1
100	NGC 1068	Sy1.9	NGC 1068	sbgr	0.004	D	0	(40.66, -0.004)	1.82	2.33	3.8	0.65	18

Table 1. *continued*

Table 1 (*continued*)

No.	<i>Swift</i> -BAT name	Type	<i>Fermi</i> -LAT name	Type	Sep. (deg)	Flag	1FLE	BAT coord. ( $\alpha_{J200}, \delta_{J2000}$ )	$\Gamma_{\text{BAT}}$	$\Gamma_{\text{LAT}}$	$F_{\text{BAT}}$	$F_{\text{LAT}}$	VarIndex
101	Circinus Galaxy	Sy2	Circinus galaxy	sey	0.01	M	0	(213.3, -65.34)	2.09	2.26	27	0.67	14
102	1H 0323+342	Beamed AGN	1H 0323+342	nlsy1	0.046	M	0	(51.21, 34.17)	1.62	2.82	2.7	1.9	2e+02
103	3C 380	Beamed AGN	3C 380	css	0.028	M	1	(277.4, 48.74)	1.52	2.42	1.5	1.8	69
104	Cas A	SNR	Cas A	snr	0.008	M	0	(350.8, 58.82)	3.33	1.97	6.5	6.2	4.5
105	Tycho SNR	SNR	Tycho	snr	0.01	M	0	(6.326, 64.14)	3.03	2.18	1.3	0.98	4.2
106	SNR G068.8+02.6	SNR	PSR J1952+3252	PSR	0.016	D	0	(298.3, 32.89)	2.27	2.28	0.92	15	6
107	SNR G21.5-00.9	SNR	PSR J1833-1034	PSR	0.01	D	0	(278.4, -10.57)	2.26	2.5	7.4	8.2	3
108	4U 1820-30	LMXB	PSR J1823-3021A	PSR	0.025	F	0	(275.9, -30.36)	5.2	2.21	95	1.4	2.6
109	SLX 1744-299	LMXB	PSR J1747-2958	PSR	0.047	F	0	(266.9, -30)	3.25	2.56	13	16	15
110	1RXS J122758.8-485343	CV	PSR J1227-4853	PSR	0.007	D	0	(187, -48.89)	1.85	2.38	3.7	2.3	74
111	PSR J1124-5916	Pulsar	PSR J1124-5916	PSR	0.054	M	0	(171.1, -59.31)	2.47	2.46	0.83	6.1	8.6
112	Vela Pulsar	Pulsar	PSR J0835-4510	PSR	0.006	M	1	(128.8, -45.18)	1.97	2.23	18	9.4e+02	4.6
113	PSR B0540-69	Pulsar	PSR J0540-6919	PSR	0.027	M	0	(85.02, -69.35)	1.93	2.47	4.9	2.8	8.1
114	2MASX J04372814-4711298	Sy1	PSR J0437-4715	PSR	0.079	F	0	(69.41, -47.21)	1.96	2.35	0.99	1.7	9.6
115	PSR J1811-1925	Pulsar	PSR J1811-1925	psr	0.014	M	0	(272.9, -19.42)	2.07	2.14	3.5	1.1	8.6
116	Crab	Pulsar	Crab Nebula <sup>†</sup>	PWN	0.003	M	0	(83.63, 22.02)	2.17	3.8	2.3e+03	16	6.1e+02
117	IGR J17461-2853	molecular cloud	PWN G0.13-0.11	pwn	0.079	F	0	(266.5, -28.89)	1.7	2.46	3.3	7	7.4
118	Cyg X-3	HMXB	Cyg X-3	HMB	0.072	M	0	(308.1, 40.96)	3.0	2.66	2.5e+02	3.5	83
119	RX J1826.2-1450	HMXB	LS 5039	HMB	0.002	M	0	(276.6, -14.85)	1.62	2.61	3.3	27	9
120	2XMM J130247.6-635008	HMXB	PSR B1259-63	HMB	0.069	M	0	(195.6, -63.85)	1.2	2.75	2	1.6	1.9e+02
121	LS I +61 303	HMXB	LSI +61 303	HMB	0.014	M	1	(40.16, 61.24)	1.73	2.38	3.2	47	2.5e+02
122	Cyg X-1	HMXB	Cyg X-1	hmb	0.035	M	0	(299.6, 35.2)	1.9	2.14	1.7e+03	0.65	12
123	V395 Car	LMXB	2S 0921-630	lmb	0.053	M	0	(140.5, -63.31)	5.38	2.23	0.56	0.19	2.7
124	Eta Carinae	HRB	Eta Carinae	BIN	0.005	M	0	(161.3, -59.68)	3.76	2.31	0.78	19	47
125	4U 2129+12	LMXB	NGC 7078	glc	0.026	F	0	(322.5, 12.17)	2.66	2.62	7.7	0.42	23
126	XB 1832-330	LMXB	NGC 6652	glc	0.015	F	0	(278.9, -32.99)	2.26	2.35	18	0.48	13
127	4U 1746-37	LMXB	NGC 6441	glc	0.021	F	0	(267.6, -37.05)	5.45	2.4	8.3	1.5	8.2
128	ESO 520-27	GC	Terzan 5	glc	0.009	M	0	(267, -24.78)	4.32	2.37	2.6	7.9	5.3
129	4U 1722-30	LMXB	Terzan 2	glc	0.049	F	0	(261.9, -30.8)	2.51	2.37	43	0.67	7.4
130	GX 340+0	LMXB	4U 1642-45	unk	0.058	U	0	(251.4, -45.61)	5.59	2.61	86	4.5	5.4
131	SAX J1808.4-3658	LMXB	(SWIFT J1808.5-3655)	unk	0.043	U	0	(272.1, -36.99)	2.34	2.44	3.7	0.44	12
132	XTE J1652-453	LMXB	(SWIFT J1652.3-4520)	unk	0.061	U	0	(253.1, -45.34)	2.51	2.58	3.1	1.9	9.2
133	PKS 2005-489	Beamed AGN	PKS 2005-489	BLL	0.088	M	0	(302.5, -48.87)	2.42	1.83	0.6	3.2	1.5e+02
134	87GB 050246.4+673341	Beamed AGN	1ES 0502+675	bil	0.094	M	0	(76.92, 67.53)	2.5	1.58	0.9	2.4	56

Table 1. *continued*

Table 1 (*continued*)

No.	<i>Swift</i> -BAT name	Type	<i>Fermi</i> -LAT name	Type	Sep. (deg)	Flag	1FLE	BAT coord. ( $\alpha_{J2000}, \delta_{J2000}$ )	$\Gamma_{\text{BAT}}$	$\Gamma_{\text{LAT}}$	$F_{\text{BAT}}$	$F_{\text{LAT}}$	VarIndex
135	2MASX J03252346-5635443	Beamed AGN	1RXS J032521.8-563543	bl	0.082	M	0	(51.47, -56.53)	2.06	1.95	0.85	0.58	36
136	PKS 0607-549	Beamed AGN	PKS 0607-549	bcu	0.137	M	0	(92.21, -55.08)	2.19	2.68	0.62	0.68	77
137	B2 0920+39	Beamed AGN	B2 0920+39	bcu	0.107	M	0	(140.8, 38.78)	1.44	2.69	1.2	0.59	91
138	8C 1849+670	Beamed AGN	S4 1849+67	FSRQ	0.087	M	0	(282.1, 67.05)	2.72	2.29	0.64	4.4	1.9e+03
139	RBS 0315	Beamed AGN	TXS 0222+185	fsrq	0.089	M	0	(36.26, 18.8)	1.73	2.95	3.1	0.5	52
140	4C +32.14	Beamed AGN	NRAO 140	fsrq	0.121	M	0	(54.12, 32.29)	1.67	2.8	4.4	1.3	46
141	PKS 2008-159	Beamed AGN	PKS 2008-159	fsrq	0.083	M	0	(302.8, -15.75)	2.41	2.82	1.3	0.48	18
142	PKS 2052-47	Beamed AGN	PKS 2052-47	fsrq	0.183	M	1	(313.8, -47.16)	2.19	2.45	1.8	6	1.3e+03
143	PKS 2145+06	Beamed AGN	PKS 2145+06	fsrq	0.142	M	0	(327, 6.936)	1.9	2.8	1.7	0.54	39
144	[HB89] 0834-201	Beamed AGN	PKS 0834-20	fsrq	0.197	M	0	(129.2, -20.25)	1.43	2.91	1.4	0.58	25
145	1RXS J174036.3+521155	Beamed AGN	4C +51.37	fsrq	0.222	M	1	(265.2, 51.97)	1.9	2.47	0.87	2.1	8e+02
146	2MASX J06230765-6436211	Beamed AGN	RX J062308.0-643619	fsrq	0.115	M	0	(95.85, -64.61)	1.98	3.04	1.2	0.25	7.9
147	87GB 162418.8+435342	Beamed AGN	MG4 J162551+4346	fsrq	0.249	M	0	(246.5, 43.81)	2.04	2.91	1.2	0.23	14
148	PKS 2331-240	Beamed AGN	PKS 2331-240	agn	0.262	M	0	(353.5, -23.69)	1.4	2.5	1.6	0.44	20
149	PKS 2153-69	Sy2	PKS 2153-69	rdg	0.125	D	0	(329.4, -69.7)	1.59	2.87	1.5	0.37	5.2
150	3C 111.0	Sy1.2	3C 111	rdg	0.1	D	1	(64.59, 38.02)	2.0	2.74	12	1.5	40
151	3C 309.1	Beamed AGN	3C 309.1	css	0.098	M	0	(224.5, 71.72)	1.8	2.5	0.77	0.43	2.1e+02
152	PSR J1420-6048	Pulsar	PSR J1420-6048	PSR	0.272	M	0	(215.3, -60.58)	2.24	2.42	1	14	14
153	PSR J1723-2837	Pulsar	PSR J1723-2837	psr	0.361	M	0	(260.8, -28.64)	0.88	2.58	1.9	0.58	12
154	CGCG 147-020	Sy2	(SWIFT J0725.8+3000)	unk	0.282	U	0	(111.4, 30.02)	2.19	1.61	0.92	0.094	15
155	2MASX J14080674-3023537	Sy1.9	(SWIFT J1408.1-3024)	unk	0.15	U	0	(212.1, -30.38)	2.16	2.59	1.6	0.24	16
156	XTE J1817-330	LMXB	(SWIFT J1817.8-3301)	unk	0.144	U	0	(274.3, -32.98)	1.65	2.5	1.8	0.22	8.8

NOTE—Flux is in units of  $10^{-11}$  erg  $\text{cm}^{-2}$   $\text{s}^{-1}$ . In 4FGL-DR2, source types with capital letters (e.g., BLL) indicate firm associations, while those with small letters (e.g., bl) are associations. The *Fermi*-LAT name in parenthesis indicate the identifications of ASSOC2 (less firm associations). No. 133–156 are matched by their names, not spatially matched.

† Crab in 4FGL-DR2 has three entries, PSR J0534+2200, Crab nebula (synchrotron radiation), and Crab nebula (IC scattering). Only the synchrotron component of the nebula is shown here.

Table 2. Cross-matched extended sources

No.	<i>Fermi</i> -LAT name	Type	LAT coord. ( $\alpha_{J2000}, \delta_{J2000}$ )	Ext. $\Gamma_{\text{LAT}}$	$F_{\text{LAT}}$	<i>Swift</i> -BAT name	Type	Sep. $\Gamma_{\text{BAT}}$	$F_{\text{BAT}}$	Flag		
			(deg)	(deg)				(deg)				
1	LMC	GAL	(80, -68.75)	3.0	2.19	11	2MASX J05052442-6734358 SWIFT J045106.8-694803 IGR J05007-7047 LMC X-4 RX J0531.2-6609 LMC X-1 PSR B0540-69 XMMU J054134.7-682550 [RSG2010] A	Unknown AGN HMXB HMXB HMXB HMXB HMXB Pulsar HMXB HMXB	1.7 2.8 2.6 2.6 2.7 2.0 1.9 2.0 1.9 2.8	2.02 2.5 2.4 2.8 2.8 2.6 1.9 2.9 2.8	1 3.3 2.2 32.7 1.35 3.21 4.93 2.42 0.566	F
2	LMC-Far West	...	(75.25, -69.75)	0.9	2.1	2	SWIFT J045106.8-694803	HMXB	0.8	2.48	3.3	F
3	LMC-30Dor West	...	(82.5, -69)	0.9	2.12	4.4	RSG2010 A	HMXB	1.0	2.82	0.57	F
4	LMC-North	...	(82.97, -66.65)	0.6	2.0	2.3	LMC X-4 RX J0531.2-6609	HMXB HMXB	0.3 0.4	2.83 2.8	33 1.35	F
5	SMC	GAL	(14.5, -72.75)	1.5	2.2	2.5	IGR J01054-7253 RX J0052.1-7319 RX J0053.8-7226 XTE J0103-728 SXP 202	HMXB HMXB HMXB HMXB HMXB	0.3 0.7 0.5 0.4 0.4	3.46 2.7 2.5 3.2 2.9	0.34 1.58 1.06 1.34 0.153	F
6	Cen A Lobes	RDG	(201, -43.5)	2.5	2.51	5.2	Cen A	Beamed AGN	0.5	1.88	1.4e+02	M
7	Vela X	PWN	(128.3, -45.19)	0.9	2.18	13	Vela Pulsar SWIFT J0837.8-4440	Pulsar U2	0.4 1.0	1.97 2.5	18 1.16	M
8	HESS J1420-607	PWN	(215.1, -60.78)	0.1	2.0	3.7	Rabbit	Pulsar	0.2	1.53	0.8	M
9	MSH 15-52	PWN	(228.6, -59.16)	0.2	1.83	5.3	PSR B1509-58	Pulsar	0.0	1.85	26	M
10	HESS J1616-508	PWN	(244.1, -50.91)	0.3	2.05	12	PSR J1617-5055	Pulsar	0.2	2.05	1.5	M
11	HESS J1825-137	PWN	(276.1, -13.85)	0.8	1.75	14	IGR J18246-1425 XMMSL1 J182155.0-134719	Pulsar HMXB	0.6 0.6	2.8 2.7	1.9 1.52	M
12	HESS J1841-055	PWN	(280.2, -5.55)	0.6	1.98	13	AX J1841.0-0535 1E 1841-045	HMXB Pulsar	0.1 0.6	1.91 1.3	2.5 10.7	M
13	HESS J1632-478	pwn	(247.9, -47.94)	0.3	1.76	3	AX J1631.9-4752	Pulsar	0.1	2.84	31	M
14	HESS J1837-069	pwn	(279.1, -6.866)	0.5	2.04	22	PSR J1838-0655	Pulsar	0.3	1.71	6.9	M
15	HESS J1837-069	pwn	(279.7, -7.067)	0.5	1.85	7	PSR J1838-0655	Pulsar	0.3	1.71	6.9	M

Table 2 continued

Table 2 (*continued*)

No.	<i>Fermi</i> -LAT name	Type	LAT coord. ( $\alpha_{J2000}, \delta_{J2000}$ )	Ext. $\Gamma_{\text{LAT}}$	(deg)	$F_{\text{LAT}}$	<i>Swift</i> -BAT name	Type	Sep. $\Gamma_{\text{BAT}}$	(deg)	$F_{\text{BAT}}$	Flag
16	SNR G150.3+04.5	SNR	(66.82, 55.55)	1.5	1.68	4.1	XTE J0421+560	HMXB	1.2	2.27	1.2	F
17	Sim 147	SNR	(85.1, 27.94)	1.5	2.18	5.7	SWIFT J053457.91+282837.9	U2	1.3	2.35	1.2	U
18	Monoceros	SNR	(99.86, 6.93)	3.5	2.3	9.1	2MASX J06262702+0727287	Unknown AGN	3.2	1.87	1.6	F
19	RX J0852.0-4622	SNR	(133, -46.34)	1.0	1.79	12	PSR J0855-4644	Pulsar	0.8	2.06	1	M
20	SNR G337.0-00.1	SNR	(249.1, -47.52)	0.1	2.34	10	SGR 1627-41	Gamma-ray source	0.1	1.81	1.4	A
							IGR J16358-4726	Pulsar	0.1	2.1	0.39	
21	gamma Cygni	SNR	(305.3, 40.52)	0.6	1.96	10	2MASX J20183871+4041003	Sy2	0.5	2.03	2.6	F
22	RX J1713.7-3946	SNR	(258.4, -39.76)	0.6	1.71	7	SWIFT J1712.9-4002	U1	0.3	3.25	1.3	M
							SNR G347.3-0.5	SNR	0.3	3.1	1.99	
23	Cygnus X	SFR	(307.2, 41.17)	3.0	2.09	1.2e+02	Cyg X-3	HMXB	0.7	3.0	2.5e+02	F
							2MASX J20183871+4041003	Sy2	1.9	2.0	2.62	
							SSTSL2 J203705.58+415005.3	Beamed AGN	1.7	5.2	1.36	
24	HESS J1632-478	spp	(248.3, -47.77)	0.6	2.17	25	AX J1631.9-4752	Pulsar	0.2	2.84	31	M
							4U 1630-47	LMXB	0.4	2.7	30.3	
							IGR J16328-4726	HMXB	0.4	3.1	2.38	
							SGR 1627-41	Gamma-ray source	0.5	1.8	1.38	
							IGR J16358-4726	Pulsar	0.6	2.1	0.39	
25	HESS J1809-193	spp	(272.6, -19.43)	0.5	2.36	5.1	PSR J1811-1925	Pulsar	0.3	2.07	3.5	A
							XTE J1810-189	LMXB	0.4	2.2	8.21	
26	HESS J1813-178	spp	(273.3, -17.62)	0.6	2.34	15	IGR J18135-1751	SNR	0.2	1.92	4.1	M
							GX 13+1	LMXB	0.6	5.7	37.9	
27	W 41	spp	(278.6, -8.78)	0.2	2.13	11	Swift J1834.9-0846	star	0.2	2.13	0.96	F
28	Kes 73	spp	(280.2, -4.89)	0.3	2.37	7.2	1E 1841-045	Pulsar	0.1	1.33	11	M
29	(FGES J1036.3-5833)	...	(159.1, -58.56)	2.5	1.93	29	Eta Carina	XR	1.6	3.76	0.78	U
							4U 1036-56	HMXB	1.8	2.7	2.82	
							2MASS J10445192-6025115	star	2.2	1.9	1.49	
30	(FGES J1409.1-6121)	...	(212.3, -61.35)	0.7	2.16	25	SWIFT J1408.2-6113	CV	0.2	2.68	1.1	U
							[CG2001] G311.45-0.13	U2	0.7	2.1	1.7	
							MAXI J1409-619	Pulsar	0.6	3.1	1.17	
31	(HESS J1808-204)	...	(272, -20.48)	0.6	2.57	4.9	SGR 1806-20	Pulsar	0.1	1.66	5.3	U

NOTE—<sup>†</sup> In 4FGL, HESS J1837-069 and HESS J1632-478 are extended and have two entries.Flux is in units of  $10^{-11}$  erg cm $^{-2}$  s $^{-1}$ . The nearest BAT source is listed at the top for the source matched with more than one BAT sources. The LAT extent of a major axis is shown here.

Table 3. Cross-match with COMPTEL sources

No.	COMPTEL	Type	Swift-BAT	Type	Fermi-LAT	Type	No. in Table 1	Note
1	PSR B1951+32	PSR	SNR G068.8+02.6	SNR	PSR J1952+3252	PSR	106	
2	PSR B0531+21	PSR	Crab	Pulsar	PSR J0534+2200	PSR	114	
3	PSR J0633+1746	PSR	...	...	PSR J0633+1746	PSR	...	Matched with only <i>Fermi</i> . Faint in the hard X-ray.
4	PSR B0656+14	PSR	...	...	PSR J0659+1414	PSR	...	Matched with only <i>Fermi</i> . Faint in the hard X-ray.
5	PSR B0833-45	PSR	Vela Pulsar	Pulsar	PSR J0835-4510	PSR	112	
6	PSR B1055-52	PSR	...	...	PSR J1057-5226	PSR	...	Matched with only <i>Fermi</i> . Faint in the hard X-ray.
7	PSR B1509-58	PSR	PSR B1509-58	Pulsar	MSH 15-52	PWN	10 in Table 2	
8	GRO J1823-12	Galactic	RX J1826.2-1450	HMXB	LS5039	HMB	120	
9	Cygnus X-1	Galactic	Cyg X-1	HMXB	Cyg X-1	hmb	123	
10	GRO J2227+61	Galactic	...	...	PSR J2229+6114	PSR	...	It has a BAT source (SWIFT J2221.6+5952) at 1.7°.
11	GT 0236+610	Galactic	LS I +61 303	HMXB	LSI +61 303	HMB	122	
12	Nova Per 1992	Galactic	...	...	...	...	...	No match. X-ray transient.
13	Crab Unpulsed	Galactic	Crab	Pulsar	PSR J0534+2200	PSR	114	
14	Vela/Carina	Galactic <sup>†</sup>	...	...	4FGL J0853.9-5501	unk	...	
15	3C 273	AGN	3C 273	Beamed AGN	3C 273	FSRQ	43	
16	3C 279	AGN	3C 279	Beamed AGN	3C 279	FSRQ	42	
17	3C 454.3	AGN	3C 454.3	Beamed AGN	3C 454.3	FSRQ	33	
18	CTA 102	AGN	[HB89] 2230+114	Beamed AGN	CTA 102	FSRQ	34	
19	Centaurus A	AGN	Cen A	Beamed AGN	Cen A	RDG	91	
20	GRO J0516-609	AGN	...	...	...	...	...	Unknown flaring source. It has a <i>Fermi</i> source (PMN J0507-6104) at 1.03°.
21	GRO J1224+2155	AGN	PG 1222+216	Beamed AGN	4C +21.35	FSRQ	44	
22	PKS 0208-512	AGN	...	...	PKS 0208-512	FSRQ	...	Matched with only <i>Fermi</i> .
23	PKS 0528+134	AGN	PKS 0528+134	Beamed AGN	PKS 0528+134	FSRQ	48	
24	PKS 1622-297	AGN	PKS 1622-29	Beamed AGN	PKS B1622-297	FSRQ	40	
25	GRO J 1753+57	Unknown <sup>†</sup>	...	...	...	...	...	No match.
26	GRO J 1040+48	Unknown	...	...	...	...	...	No match.
27	GRO J 1214+06	Unknown	2MASX J12150077+0500512	Sy1.8	(SDSS J12168+0541)	(unk)	...	Association?

NOTE—<sup>†</sup> Extended.





**Table 4.** Classes of cross-matched sources (*Swift*-BAT definition)

Source	Original		Matched point sources		Extended		ID-matched		Total-matched			
	#	%	#	Firm	#	Firm	#	Firm	#	%	Firm #	Firm %
Total	1632		132	115	31	15	24	21	187		151	
Beamed AGN	158	9.7	89	89	1	1	17	17	107	57.2	107	70.9
Starburst galaxy	1	0.1	1	1	0	0	0	0	1	0.5	1	0.7
Seyfert galaxy	827	50.7	10	6	1	0	4	2	15	8.0	8	5.3
LINER	6	0.4	0	0	0	0	0	0	0	0.0	0	0.0
Unknown AGN	114	7.0	1	0	2	0	0	0	3	1.6	0	0.0
Compact group of galaxies	1	0.1	0	0	0	0	0	0	0	0.0	0	0.0
Galaxy Cluster	26	1.6	0	0	0	0	0	0	0	0.0	0	0.0
Galactic Center	1	0.1	1	1	0	0	0	0	1	0.5	1	0.7
HMXB	108	6.6	5	5	6	0	0	0	11	5.9	5	3.3
LMXB	109	6.7	10	1	0	0	1	0	11	5.9	1	0.7
XRB	8	0.5	1	1	1	0	0	0	2	1.1	1	0.7
Pulsar	25	1.5	5	5	14	12	2	2	21	11.2	19	12.6
SNR	7	0.4	4	4	2	2	0	0	6	3.2	6	4.0
Nova	6	0.4	0	0	0	0	0	0	0	0.0	0	0.0
CV	75	4.6	1	1	1	0	0	0	2	1.1	1	0.7
Symbiotic star	4	0.3	0	0	0	0	0	0	0	0.0	0	0.0
star	12	0.7	0	0	1	0	0	0	1	0.5	0	0.0
Open star cluster	1	0.1	0	0	0	0	0	0	0	0.0	0	0.0
molecular cloud	2	0.1	1	0	0	0	0	0	1	0.5	0	0.0
GC	1	0.1	1	1	0	0	0	0	1	0.5	1	0.7
Gamma-ray source	1	0.1	0	0	1	0	0	0	1	0.5	0	0.0
confused source	10	0.6	1	0	0	0	0	0	1	0.5	0	0.0
U1	36	2.2	0	0	0	0	0	0	0	0.0	0	0.0
U2	55	3.4	0	0	1	0	0	0	1	0.5	0	0.0
U3	38	2.3	1	0	0	0	0	0	1	0.5	0	0.0

NOTE— Firm matches indicate sources with Flag being M or D, and do not include false-matched, unidentified, and ambiguous sources for safety. The nearest source was used for the counterpart of the extended Fermi sources. Here Seyfert galaxy includes all Seyfert 1 and 2 types.

**Table 5.** Classes of cross-matched sources (4FGL-DR2 definition)

Source	Original		Matched point sources		Extended		ID-matched		Total-matched			
	#	%	#	Firm	#	Firm	#	Firm	#	%	Firm #	Firm %
Total	5788		132	115	31	15	24	21	187		151	
BLL	1190	21	32	30	0	0	3	3	35	18.7	33	21.9
FSRQ	730	13	43	40	0	0	10	10	53	28.3	50	33.1
BCU	1517	26	14	13	0	0	2	2	16	8.6	15	9.9
AGN	11	0.19	1	1	0	0	1	1	2	1.1	2	1.3
RDG	44	0.76	7	7	1	1	2	2	10	5.3	10	6.6
SBG	8	0.14	3	3	0	0	0	0	3	1.6	3	2.0
SEY	1	0.017	1	1	0	0	0	0	1	0.5	1	0.7
NLSY1	9	0.16	1	1	0	0	0	0	1	0.5	1	0.7
css	5	0.086	1	1	0	0	1	1	2	1.1	2	1.3
ssrq	2	0.035	0	0	0	0	0	0	0	0.0	0	0.0
GAL	5	0.086	0	0	2	0	0	0	2	1.1	0	0.0
SNR	43	0.74	2	2	7	2	0	0	9	4.8	4	2.6
PSR	259	4.5	10	7	0	0	2	2	12	6.4	9	6.0
PWN	18	0.31	2	1	9	9	0	0	11	5.9	10	6.6
spp	95	1.6	0	0	5	3	0	0	5	2.7	3	2.0
BIN	9	0.16	1	1	0	0	0	0	1	0.5	1	0.7
HMB	8	0.14	5	5	0	0	0	0	5	2.7	5	3.3
LMB	4	0.069	1	1	0	0	0	0	1	0.5	1	0.7
glc	30	0.52	5	1	0	0	0	0	5	2.7	1	0.7
SFR	5	0.086	0	0	1	0	0	0	1	0.5	0	0.0
NOV	1	0.017	0	0	0	0	0	0	0	0.0	0	0.0
unidentified	1794	31	3	0	6	0	3	0	12	6.4	0	0.0

NOTE— Firm matches indicate sources with Flag being M or D, and do not include false-matched, unidentified, and ambiguous sources for safety.